

FTUAM 09/5
IFT-UAM/CSIC-09-17
FTPI-MINN-09-14
UMN-TH-2742/09

26 March 2009

Right-handed sneutrino dark matter in the NMSSM

David G. Cerdeño ¹, Osamu Seto ²

¹ *Departamento de Física Teórica C-XI, and Instituto de Física Teórica UAM-CSIC,
Universidad Autónoma de Madrid, Cantoblanco, E-28049 Madrid, Spain*

² *William I. Fine Theoretical Physics Institute,
University of Minnesota, Minneapolis, MN 55455, USA*

Abstract

We study the properties of the right-handed sneutrino and its viability as a WIMP dark matter candidate in an extended version of the NMSSM in which a right-handed neutrino superfield is included with a coupling to the singlet Higgs in order to provide non-vanishing Majorana neutrino masses. We perform a systematic study of the parameter space, including LEP constraints and experimental bounds on low-energy observables. We investigate the conditions under which the right-handed sneutrino has the correct relic abundance and the dominant annihilation channels. Next we calculate the theoretical predictions for the sneutrino-proton elastic scattering cross section and compare it with present and future experimental sensitivities. We find that sneutrinos with a mass in the range of 5-200 GeV can reproduce the observed dark matter relic density without being excluded by direct dark matter searches and for natural values of the input parameters. Interestingly, the predicted scattering cross section is generally within the reach of future experiments. Finally, we comment on the possible implications for collider physics.

1 Introduction

A number of astrophysical and cosmological observations have provided substantial evidence supporting the existence of dark matter, an abundant component of our Universe made of some new, yet undiscovered, particles. A generic weakly interacting massive particle (WIMP) is one of the most promising and attractive candidates for cold dark matter in our Universe [1], since it would be thermally produced in sufficient amount to account for the observed dark matter density. Interestingly, WIMPs appear in many well motivated extensions of the standard model providing new physics at the TeV scale, such as supersymmetry (SUSY).

In supersymmetric models a discrete symmetry (R-parity) is often imposed in order to forbid lepton and baryon violating processes which could lead, for instance, to rapid proton decay. A remarkable phenomenological consequence is that supersymmetric particles can only be produced or annihilate in pairs, thus rendering the lightest SUSY particle (LSP) stable. If it is neutral and weakly interacting, the LSP can therefore be an excellent WIMP candidate for dark matter. Two particles exist with these properties in the minimal supersymmetric standard model (MSSM), namely the lightest neutralino [2, 3] and the sneutrino [4]. The former is the mixture of neutral gauginos and Higgsinos, and one of the most popular and well studied dark matter candidates [5]. In contrast, the (left-handed) sneutrino in the MSSM turns out not to be viable as dark matter. Being a left-handed field, the sneutrino has a sizable coupling with the Z boson, which entails a too large annihilation cross section and therefore a too small relic abundance. Furthermore, its scattering cross section off nuclei, also mediated by Z boson exchange, is so large that direct detection experiments for dark matter would have already observed it [6]. It should be noted that the inclusion of a lepton number violating operator can reduce the detection rate [7]. A re-analysis of the sneutrino LSP in the MSSM in light of an updated data can be found in Ref. [8].

There are motivations to consider extensions of the MSSM. One of them is the observation of neutrino oscillation phenomena, suggested by the solar and atmospheric neutrino anomalies and confirmed by various experiments [9], which imply non-vanishing (albeit very small) neutrino masses. However, in the MSSM as well as the SM, neutrinos are massless and the tiny neutrino mass is usually explained by a see-saw mechanism in which right-handed Majorana neutrinos, N , are introduced [10] with a large Majorana mass (usually taken to be around the grand unification scale, but which can also be of order of the electroweak scale or even lower).

In supersymmetric models, at same time, one has to introduce right-handed sneutrinos, which would then mix with the left-handed sneutrinos. Interestingly, a mixed left- and right-handed sneutrino has a reduced coupling to the Z boson thereby alleviating the abovementioned problems and making it viable as dark matter [11, 12]. However, a significant left-right mixture is only possible in some particular supersymmetry breaking schemes with a large trilinear term [11, 13]. Such a mechanism is not available in the standard supergravity mediated supersymmetry breaking, where trilinear terms are proportional to the small neutrino Yukawa couplings. Recently, another realization of large mixing was pointed out [14] by abandoning the canonical see-saw formula [10] for neutrino masses. Another possibility is having a pure right-handed sneutrino [15, 16, 17, 18, 19, 20, 21, 22, 23]. These cannot be thermal relics, since their coupling to ordinary matter is extremely reduced by the neutrino Yukawa coupling [15, 16, 17, 18], unless they are somehow coupled to the observable sector, for example via an extension of the gauge [19, 20] or Higgs [21, 22, 23] sectors¹.

The other motivation to extend the MSSM is the so-called “ μ problem” [25]. The superpotential in the MSSM contains a bilinear term $\mu H_1 H_2$ which gives supersymmetric Higgs/Higgsino mass terms. Successful radiative electroweak symmetry breaking (REWSB) [26] requires μ of the order of the electroweak scale. The next-to minimal supersymmetric standard model (NMSSM) addresses this problem in a very natural way. A new singlet superfield, S , is introduced [27] and the bilinear term (forbidden by a global Z_3 symmetry) is promoted to a trilinear coupling $\lambda S H_1 H_2$. Once REWSB takes place the singlet field acquires a vacuum expectation value (VEV), $v_s = \langle S \rangle$, thereby generating an effective μ parameter, $\mu = \lambda v_s$. The NMSSM also alleviates the “little hierarchy problem” of the Higgs sector in the MSSM [28]. Due to the significant changes in the Higgs and neutralino sectors, the NMSSM also has an attractive phenomenology [29] and interesting consequences for neutralino dark matter [30, 31, 32]. Notice finally that although the Z_3 symmetry of the NMSSM may give rise to a cosmological domain wall problem, this can be avoided with the inclusion of non-renormalisable operators [33, 34].

Motivated by above two issues, in Ref. [22] an extension of the MSSM was proposed in which two new singlet superfields were included, as in Refs. [35, 21]. An extra singlet superfield S addresses the μ problem in the same way as in the NMSSM and provides extra Higgs and neutralino states, while an extra singlet superfield N accounts for right-handed neutrino and sneutrino states. This model possesses two interesting

¹Recently, non-LSP right-handed sneutrino dark matter model was also proposed [24].

new consequences. The right-handed neutrino mass is generated spontaneously (or dynamically) with the electroweak symmetry breaking. Due to the non-vanishing VEV of the singlet Higgs, an effective Majorana mass for the right-handed neutrino appears through the new coupling $SN\bar{N}$ which is of order of the electroweak scale, in the same way as the effective μ term is generated in the NMSSM. Moreover, the singlet S , which couples to the MSSM Higgs sector, provides electroweak scale interactions of the right-handed sneutrino with the rest of the MSSM fields. Thus, the purely right-handed sneutrino LSP has the properties of a WIMP. In Ref. [22] it was shown that right-handed sneutrinos in this construction can not only be thermally produced in sufficient amount to account for the dark matter in the Universe but also that their elastic scattering cross section with nuclei is large enough to detect them through Higgs exchange processes.

In this work we perform a systematic analysis of the properties of the right-handed sneutrino as a dark matter candidate in the model of Ref. [22]. In Section 2 the theoretical details of this construction are introduced, explaining in detail the properties of the sneutrino spectrum. In Section 3 the thermal production of right-handed sneutrinos is analysed for several examples in the parameter space. The right-handed sneutrino relic abundance is calculated and the importance of the different annihilation channels is investigated in detail. In Section 4 the direct detection properties of the right-handed sneutrino are studied, comparing the theoretical predictions of its elastic scattering cross section off nuclei with present and future experimental sensitivities. In Section 5 we briefly comment on the possible implications of this model for collider physics, describing the characteristic signals that could be expected. In Section 6 we summarize our conclusions. The technical details are relegated to the Appendices. In Appendix A we include the Feynman rules for the new diagrams of the model, and in Appendix B we detail the calculation of the sneutrino relic abundance and give the explicit expressions for the different annihilation channels.

2 The Model

The model consists of an extended version of the NMSSM with a new singlet right-handed neutrino superfield N . The superpotential is therefore given by

$$W = W_{\text{NMSSM}} + \lambda_N S N \bar{N} + y_N L \cdot H_2 N, \quad (2.1)$$

$$W_{\text{NMSSM}} = Y_u H_2 \cdot Q u + Y_d H_1 \cdot Q d + Y_e H_1 \cdot L e - \lambda S H_1 \cdot H_2 + \frac{1}{3} \kappa S^3, \quad (2.2)$$

where flavour indices are omitted and the dot denotes the $SU(2)_L$ antisymmetric product. As in the NMSSM, a global Z_3 symmetry is imposed for each superfield, so that there are no supersymmetric mass terms in the superpotential. Note that the term NNN and SSN are gauge invariant but not consistent with R-parity and thus are not included. Notice also that N does not have a bare Majorana mass but acquires a mass through the non-vanishing singlet Higgs VEV, v_s .

The supersymmetric scalar potential for squarks, sleptons, Higgses and the right-handed sneutrino, \tilde{N} , is given as $V = V_F + V_D$ with

$$\begin{aligned}
V_F = & |Y_u H_2 \tilde{u} + Y_d H_1 \tilde{d}|^2 + |Y_u H_2 \tilde{Q}|^2 + |Y_d H_1 \tilde{Q}|^2 + |Y_e H_1 \tilde{e} + y_N H_2 \tilde{N}|^2 + |Y_e H_1 \tilde{L}|^2 \\
& + |Y_d \tilde{Q} \tilde{d} + y_N \tilde{L} \tilde{e} - \lambda S H_2|^2 + |Y_u \tilde{Q} \tilde{u} - \lambda S H_1 + y_N \tilde{L} \tilde{N}|^2 \\
& + |-\lambda H_1 H_2 + \kappa S^2 + \lambda_N \tilde{N}^2|^2 + |2\lambda_N S \tilde{N} + y_N \tilde{L} H_2|^2,
\end{aligned} \tag{2.3}$$

and

$$\begin{aligned}
V_D = & \frac{g_1^2}{2} \left(H_1^\dagger \frac{-1}{2} H_1 + H_2^\dagger \frac{1}{2} H_2 + \tilde{Q}^\dagger \frac{1}{6} \tilde{Q} + \tilde{u}^\dagger \frac{-1}{3} \tilde{u} + \tilde{d}^\dagger \frac{1}{3} \tilde{d} + \tilde{L}^\dagger \frac{-1}{2} \tilde{L} + \tilde{e}^\dagger \tilde{e} \right)^2 \\
& + \frac{g_2^2}{2} \sum_a \left(H_1^\dagger \frac{\tau^a}{2} H_1 + H_2^\dagger \frac{\tau^a}{2} H_2 + \tilde{Q}^\dagger \frac{\tau^a}{2} \tilde{Q} + \tilde{L}^\dagger \frac{\tau^a}{2} \tilde{L} \right)^2.
\end{aligned} \tag{2.4}$$

The soft SUSY breaking terms are

$$\begin{aligned}
-\mathcal{L}_{\text{scalar mass}} = & m_{\tilde{Q}}^2 |\tilde{Q}|^2 + m_{\tilde{u}}^2 |\tilde{u}|^2 + m_{\tilde{d}}^2 |\tilde{d}|^2 + m_{\tilde{L}}^2 |\tilde{L}|^2 + m_{\tilde{e}}^2 |\tilde{e}|^2 \\
& + m_{H_1}^2 |H_1|^2 + m_{H_2}^2 |H_2|^2 + m_S^2 |S|^2 + m_{\tilde{N}}^2 |\tilde{N}|,
\end{aligned} \tag{2.5}$$

where the new soft scalar masses $m_{\tilde{N}}$ and m_S are included, and

$$\begin{aligned}
-\mathcal{L}_{\text{A-terms}} = & \left(A_u Y_u H_2 \tilde{Q} \tilde{u} + A_d Y_d H_1 \tilde{Q} \tilde{d} + A_e Y_e H_1 \tilde{L} \tilde{e} + \text{H.c.} \right) \\
& + \left(-\lambda A_\lambda S H_1 H_2 + \frac{1}{3} \kappa A_\kappa S^3 + \text{H.c.} \right) \\
& + \left(\lambda_N A_{\lambda_N} S \tilde{N}^2 + y_N A_{y_N} \tilde{L} H_2 \tilde{N} + \text{H.c.} \right),
\end{aligned} \tag{2.6}$$

which contains the new trilinear soft terms A_{λ_N} and A_{y_N} . The sum of the supersymmetric and soft SUSY breaking terms give the total scalar potential.

2.1 Neutrino mass

As stated above, in this construction, right-handed neutrino masses are generated by the non-vanishing VEV of the singlet Higgs as

$$M_N = 2\lambda_N v_s, \tag{2.7}$$

being therefore of order of the electroweak scale. Then, in order to reproduce the small masses of the left-handed neutrinos, which are given as

$$m_{\nu_L} = \frac{y_N^2 v_2^2}{M_N}, \quad (2.8)$$

the low scale seesaw mechanism implies small Yukawa couplings of $\mathcal{O}(10^{-6})$ or less. Here, $v_{1,2} = \langle H_{1,2} \rangle$ denote the VEV of the Higgs doublet. To reproduce light neutrino masses and mixing for neutrino oscillation data we would need to introduce the generation structure in the right-handed neutrino sector. However, as we will see, these small neutrino Yukawa couplings are completely irrelevant for dark matter physics. Hence, for simplicity, we consider one generation case, but one may regard that the considered sneutrino corresponds to the lightest one among multi-generations.

2.2 Sneutrino masses

The sneutrino mass matrix can be read from the quadratic terms with respect to \tilde{L} and \tilde{N}

$$\begin{aligned} V(\tilde{L}, \tilde{N}) \subset & |y_N H_2 \tilde{N}|^2 + |2\lambda_N S \tilde{N}|^2 + |-\lambda S H_1 + y_N \tilde{L} \tilde{N}|^2 \\ & + |-\lambda H_1 H_2 + \kappa S^2 + \lambda_N \tilde{N}^2|^2 + \text{D-term} \\ & + m_{\tilde{L}}^2 |\tilde{L}|^2 + m_{\tilde{N}}^2 |\tilde{N}|^2 + \left(\lambda_N A_{\lambda_N} S \tilde{N}^2 + y_N A_{y_N} \tilde{L} H_2 \tilde{N} + \text{H.c.} \right). \end{aligned} \quad (2.9)$$

Decomposing the left-handed sneutrino $\tilde{\nu}_L$ and right-handed sneutrino \tilde{N} as

$$\tilde{\nu}_L \equiv \frac{1}{\sqrt{2}}(\tilde{\nu}_{L1} + i\tilde{\nu}_{L2}), \quad \tilde{N} \equiv \frac{1}{\sqrt{2}}(\tilde{N}_1 + i\tilde{N}_2), \quad (2.10)$$

the sneutrino quadratic term can be written as

$$\frac{1}{2}(\tilde{\nu}_{L1}, \tilde{N}_1, \tilde{\nu}_{L2}, \tilde{N}_2) \mathcal{M}_{\text{Sneutrino}}^2 \begin{pmatrix} \tilde{\nu}_{L1} \\ \tilde{N}_1 \\ \tilde{\nu}_{L2} \\ \tilde{N}_2 \end{pmatrix}, \quad (2.11)$$

with

$$\mathcal{M}_{\text{Sneutrino}}^2 = \begin{pmatrix} m_{L\tilde{L}}^2 & \frac{m_{LR}^2 + m_{L\bar{R}}^2 + \text{c.c.}}{2} & 0 & i \frac{m_{LR}^2 - m_{L\bar{R}}^2 - \text{c.c.}}{2} \\ \frac{m_{LR}^2 + m_{L\bar{R}}^2 + \text{c.c.}}{2} & m_{R\bar{R}}^2 + m_{RR}^2 + m_{RR}^{2*} & i \frac{m_{LR}^2 - m_{L\bar{R}}^2 - \text{c.c.}}{2} & i(m_{RR}^2 - m_{RR}^{2*}) \\ 0 & i \frac{m_{LR}^2 - m_{L\bar{R}}^2 - \text{c.c.}}{2} & m_{L\tilde{L}}^2 & \frac{-m_{LR}^2 + m_{L\bar{R}}^2 + \text{c.c.}}{2} \\ i \frac{m_{LR}^2 - m_{L\bar{R}}^2 - \text{c.c.}}{2} & i(m_{RR}^2 - m_{RR}^{2*}) & \frac{-m_{LR}^2 + m_{L\bar{R}}^2 + \text{c.c.}}{2} & m_{R\bar{R}}^2 - m_{RR}^2 - m_{RR}^{2*} \end{pmatrix}.$$

(2.12)

Here, we defined

$$\begin{aligned}
m_{L\bar{L}}^2 &\equiv m_{\tilde{L}}^2 + |y_N v_2|^2 + \text{D-term}, \\
m_{LR}^2 &\equiv y_N (-\lambda v_s v_1)^\dagger + y_N A_N v_2, \\
m_{L\bar{R}}^2 &\equiv y_N v_2 (-\lambda v_s)^\dagger, \\
m_{R\bar{R}}^2 &\equiv m_{\tilde{N}}^2 + |2\lambda_N v_s|^2 + |y_N v_2|^2, \\
m_{RR}^2 &\equiv \lambda_N (A_{\lambda_N} v_s + (\kappa v_s^2 - \lambda v_1 v_2)^\dagger).
\end{aligned} \tag{2.13}$$

If these are real, in other words no CP violation, the real part and imaginary part of sneutrinos do not mix and its mass matrix (2.11) is simplified as

$$\begin{aligned}
\text{Eq. (2.11)} &= \frac{1}{2}(\tilde{\nu}_{L1}, \tilde{N}_1) \begin{pmatrix} m_{L\bar{L}}^2 & m_{LR}^2 + m_{L\bar{R}}^2 \\ m_{LR}^2 + m_{L\bar{R}}^2 & m_{R\bar{R}}^2 + 2m_{RR}^2 \end{pmatrix} \begin{pmatrix} \tilde{\nu}_{L1} \\ \tilde{N}_1 \end{pmatrix} \\
&+ \frac{1}{2}(\tilde{\nu}_{L2}, \tilde{N}_2) \begin{pmatrix} m_{L\bar{L}}^2 & -m_{LR}^2 + m_{L\bar{R}}^2 \\ -m_{LR}^2 + m_{L\bar{R}}^2 & m_{R\bar{R}}^2 - 2m_{RR}^2 \end{pmatrix} \begin{pmatrix} \tilde{\nu}_{L2} \\ \tilde{N}_2 \end{pmatrix}.
\end{aligned} \tag{2.14}$$

Note that the mixing between left-handed and right-handed sneutrinos is induced by m_{LR}^2 and $m_{L\bar{R}}^2$, both of which are proportional to the neutrino Yukawa coupling y_N . As mentioned in the previous subsection, y_N must be as small as $\mathcal{O}(10^{-(6-7)})$ to generate sub-eV left-handed neutrino mass via low scale seesaw mechanism according to Eq. (2.8). If we rewrite sneutrinos in the mass eigenstates,

$$\tilde{\nu}_i = N_{i\tilde{\nu}_L}^{\tilde{\nu}} \tilde{\nu}_L + N_{i\tilde{N}}^{\tilde{\nu}} \tilde{N}, \tag{2.15}$$

by rotating with an unitary matrix $N^{\tilde{\nu}}$, then, unless the diagonal elements of the mass matrix (2.14) are extremely degenerated, we find

$$(N_{i\tilde{\nu}_L}^{\tilde{\nu}}, N_{i\tilde{N}}^{\tilde{\nu}}) = \begin{cases} (1 + \mathcal{O}(y_N), \mathcal{O}(y_N)) \\ (\mathcal{O}(y_N), 1 + \mathcal{O}(y_N)) \end{cases}. \tag{2.16}$$

Thus, the mixing between left-handed and right-handed sneutrinos is also of $\mathcal{O}(10^{-6} - 10^{-7})$ and therefore negligible. For all practical purposes in this paper, we can ignore all off-diagonal elements in Eq. (2.14) and regard sneutrino mass eigenstates as pure left- or right-handed fields. One may see that m_{RR}^2 splits the masses of \tilde{N}_1 and \tilde{N}_2 . In particular, \tilde{N}_2 is heavier than \tilde{N}_1 for $m_{RR}^2 < 0$ (and viceversa), and this is the situation we will consider throughout the rest of this work².

²We only do this for simplicity. The imaginary component of the right-handed sneutrino is as good a dark matter candidate as the real component. In fact they only differ in the expression for the annihilation into a pair of right-handed neutrinos.

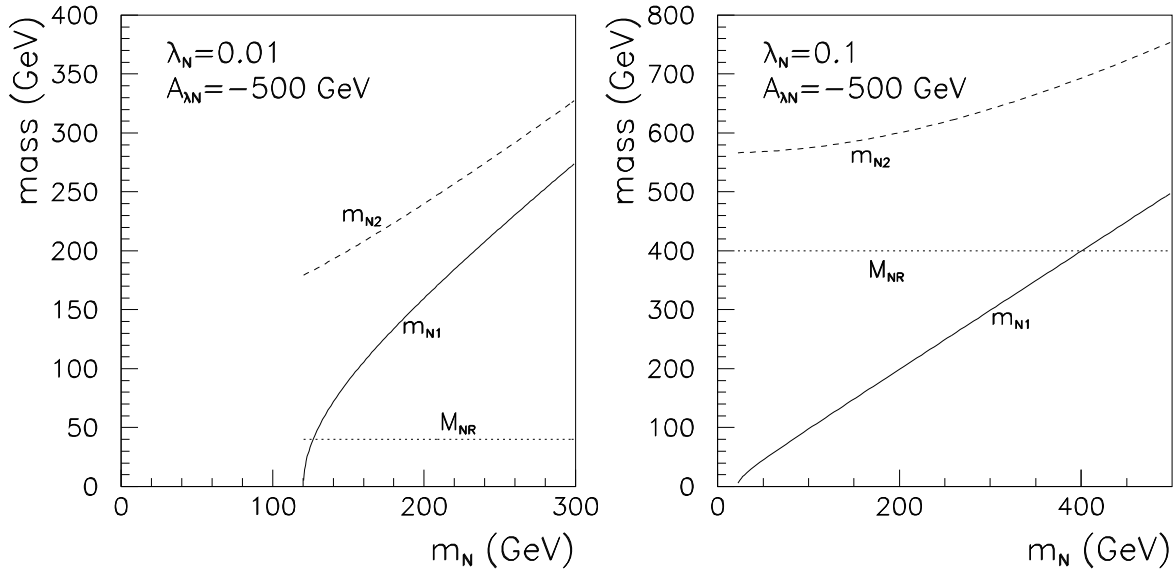


Figure 1: Sneutrino spectrum and right-handed neutrino mass, M_N , as a function of the sneutrino soft mass $m_{\tilde{N}}$ for $A_{\lambda_N} = -500$ GeV and $\lambda_N = 0.01, 0.05$. The NMSSM parameters have been chosen as $\lambda = 0.1$, $\kappa = 0.05$, $\tan \beta = 5$, and $\mu = 200$ GeV.

Let us briefly illustrate these properties of the sneutrino spectrum. As an explicit example, we have taken $\mu = 200$ GeV and $\lambda = 0.1$ (which implies $v_s = 2000$ GeV), $\kappa = 0.05$, together with $\tan \beta = 5$, $A_\lambda = 400$ GeV, and $A_\kappa = 0$. We fix $A_{\lambda_N} = -500$ GeV and consider two cases, with $\lambda_N = 0.01$ and 0.1 . From Eq. (2.7) the right-handed neutrino mass can be calculated to be $M_N = 40$ GeV, and 400 GeV, respectively. The sneutrino masses are then an increasing function of $m_{\tilde{N}}$. These features are displayed in Fig. 1, where the resulting sneutrino masses are plotted, together with the right-handed neutrino mass, as a function of $m_{\tilde{N}}$.

As commented above, the mass-splitting of the two sneutrino mass eigenstates is dictated by the m_{RR}^2 term in Eq. (2.13). An increase in λ_N implies not only an enhancement of M_N in Eq. (2.7), but also leads to a larger mass difference between \tilde{N}_1 and \tilde{N}_2 through the increase in $|m_{RR}^2|$. This is clearly evidenced in the two panels of Fig. 1. Notice that although the neutrino Majorana mass, M_N , always contributes to the sneutrino mass through the m_{RR}^2 term in Eq. (2.13), the negativeness of the m_{RR}^2 term allows sneutrinos lighter than right-handed neutrinos.

Variations in κ and A_{λ_N} have no impact on the right-handed neutrino mass, but affect the mass splitting of sneutrino states through their contribution to the m_{RR}^2

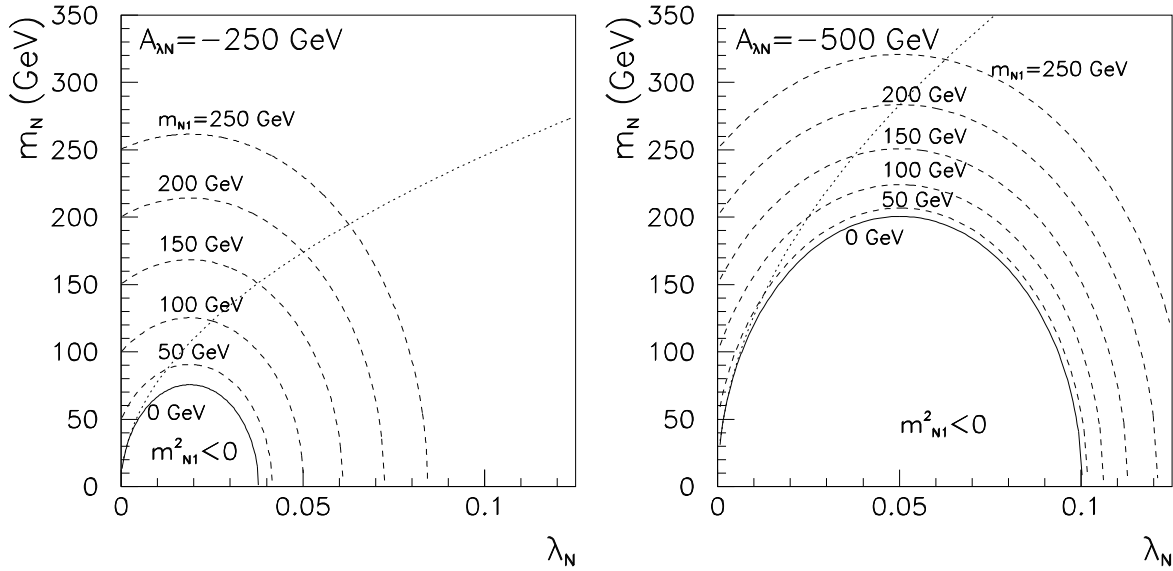


Figure 2: $(m_{\tilde{N}}, \lambda_N)$ plane for the same example as in Fig. 1 but with $A_\lambda = 250$ GeV (left) and 500 GeV (right). The trajectories with a fixed sneutrino mass are indicated by means of dashed lines. The dotted line represents the trajectory along which the sneutrino mass equals the right-handed neutrino mass (above that line, $m_{\tilde{N}_1} > M_N$).

term in Eq. (2.13). Depending on the relative signs of the various terms in this expressions, variations in κ and A_{λ_N} can enhance or decrease the lightest sneutrino mass, respectively.

In order to illustrate the effect of the A_{λ_N} parameter, we have represented in Fig. 2 the trajectories in the $(m_{\tilde{N}}, \lambda_N)$ plane with a fixed sneutrino mass for $A_{\lambda_N} = -250$ GeV and -500 GeV. For a given value of the sneutrino mass a larger $|A_{\lambda_N}|$ allows a wider range of values of λ_N . We will later use this flexibility in order to look for regions in the parameter space with the correct relic abundance.

Variations in λ and κ also alter the allowed range of values for λ_N given a fixed sneutrino mass, since they affect the m_{RR}^2 term. In general, an increase (decrease) in $|\lambda|$ ($|\kappa|$) leads to a larger $|m_{RR}^2|$ and therefore to a larger range in λ_N , with an effect that mimics the increase in $|A_{\lambda_N}|$ discussed above³. Notice also that, for a given $\mu = \lambda v_s$,

³Remember in this sense that we are concentrating on the case $m_{RR}^2 < 0$, which leads to the real component of the sneutrino to be the lightest particle. In the opposite case, $m_{RR}^2 > 0$, when the lightest component is the imaginary one, the range in λ_N would be enlarged for a decrease (increase) in $|\lambda|$ ($|\kappa|$), again due to the enhancement of $|m_{RR}^2|$.

an increase in $|\lambda|$ entails a reduction of the right-handed neutrino mass through the decrease in v_s . This makes it easier to obtain sneutrinos with a mass larger than the right-handed neutrino, which might be welcome in order to obtain the correct relic abundance as we will see in the next section.

For completeness, we display in Fig. 3 the contours with a constant sneutrino mass in the (λ, κ) plane for a specific choice of λ_N , $m_{\tilde{N}}$, and A_{λ_N} . As $|\lambda|$ ($|\kappa|$) increases (decreases), the splitting between the two right-handed sneutrino states (real and imaginary components) decreases and at some point they become degenerate. This is indicated by means of a dashed line in the plot. For our choice of parameters the real component of the right-handed sneutrino is the light state below that line and the imaginary component becomes lighter in the region above. Notice that (depending on the values of the input parameters) the sneutrino can become tachyonic (e.g., for small values of κ or small values of λ). Obviously, the tachyonic regions are larger for a smaller sneutrino soft mass.

Finally, despite the importance of variations of $\tan\beta$ in the NMSSM phenomenology, they only affect the term $v_1 v_2$ in Eq. (2.13), which is proportional to $\tan\beta/(1 + \tan^2\beta)$ and have therefore little impact on the resulting right-handed sneutrino spectrum.

2.3 Vacuum and Higgs potential

So far, we have assumed that $\langle \tilde{N} \rangle = 0$ holds in the vacuum. However, the right-handed sneutrino may have a non vanishing VEV, depending on the specific choice of parameters [35]. We will check here the validity of that assumption and the implications for the relevant parameters of the model.

The part of the scalar potential related with Higgses and sneutrinos is given by

$$\begin{aligned}
V = & |y_N H_2 \tilde{N}|^2 + |\lambda S H_2|^2 + |\lambda S H_1|^2 + |-\lambda H_1 H_2 + \kappa S^2 + \lambda_N \tilde{N}^2|^2 + |2\lambda_N S \tilde{N}|^2 \\
& + V_D(H_1, H_2) \\
& + m_{H_1}^2 |H_1|^2 + m_{H_2}^2 |H_2|^2 + m_S^2 |S|^2 + m_{\tilde{N}}^2 |\tilde{N}|^2 \\
& + \left(-\lambda A_\lambda S H_1 H_2 + \frac{1}{3} \kappa A_\kappa S^3 + \lambda_N A_{\lambda_N} S \tilde{N}^2 + \text{H.c.} \right). \tag{2.17}
\end{aligned}$$

As showed in the previous subsection, the left-handed and right-handed sneutrinos are almost decoupled from each other. Thus, for this discussion, only right-handed

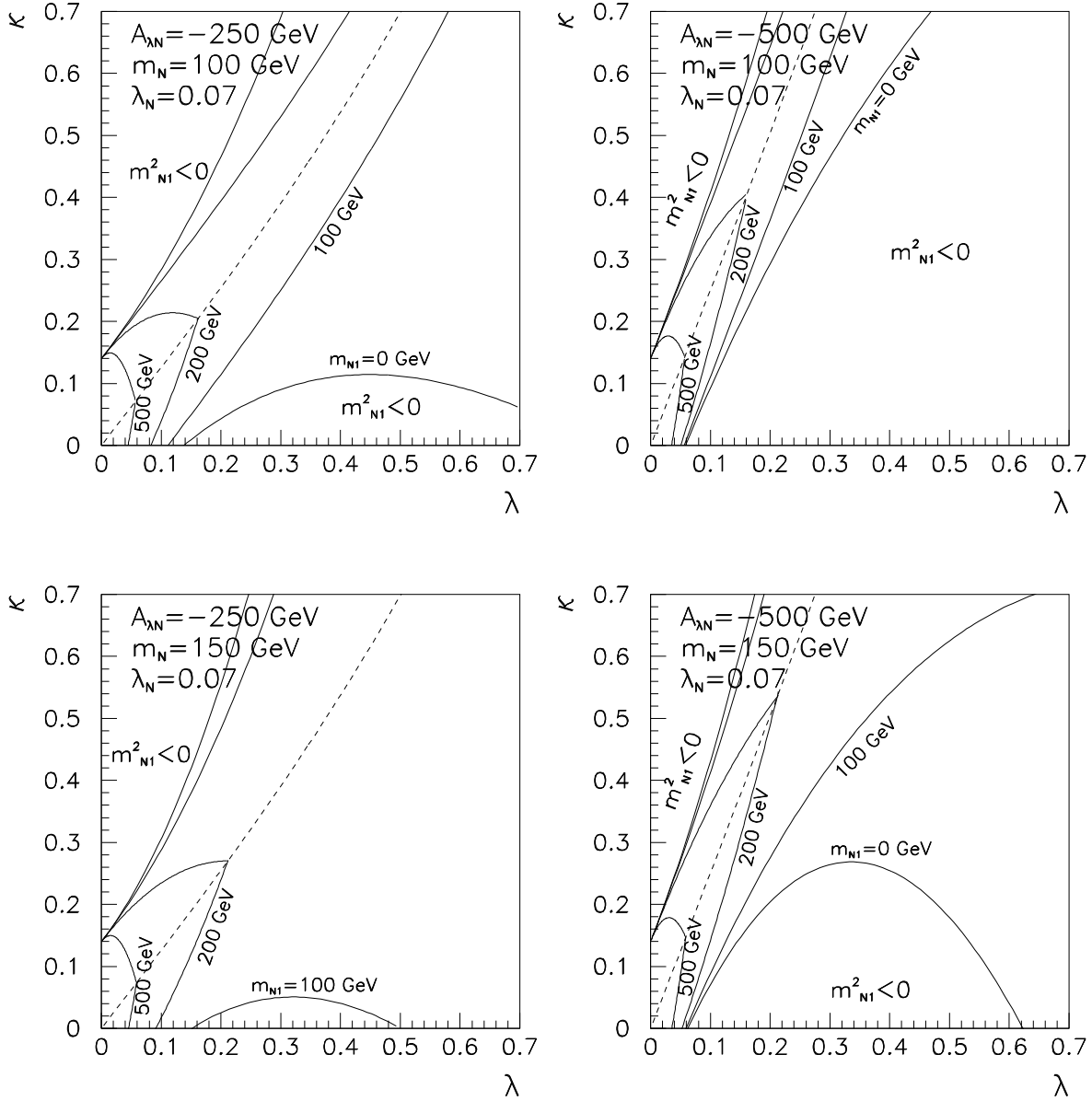


Figure 3: Trajectories for constant sneutrino mass in the (λ, κ) plane the same case described in Fig.1 and the choices $\lambda_N = 0.07$, $m_{\tilde{N}} = 100, 150$ GeV and $A_{\lambda_N} = 250, 500$ GeV. Below the dotted line, the lightest right-handed sneutrino corresponds to the real component, whereas the imaginary component becomes lighter in regions above that line.

sneutrinos are relevant. From the stationary condition

$$\begin{aligned}
\frac{\partial V}{\partial \tilde{N}} &= 2\lambda_N(-\lambda H_1 H_2 + \kappa S^2)^* \tilde{N} + 2|\lambda_N|^2 |\tilde{N}|^2 \tilde{N}^* \\
&\quad + (|2\lambda_N S|^2 + m_{\tilde{N}}^2 + |y_N H_2|^2) \tilde{N}^* + 2\lambda_N A_{\lambda_N} S \tilde{N} \\
&= \tilde{N}^* \left[m_{R\bar{R}}^2 + 2|\lambda_N|^2 |\tilde{N}|^2 + (2\lambda_N(-\lambda H_1 H_2 + \kappa S^2))^* + 2\lambda_N A_{\lambda_N} S \right] \left(\frac{\tilde{N}}{\tilde{N}^*} \right) \\
&= 0,
\end{aligned} \tag{2.18}$$

the possible minimum or maximum is given by

$$|\langle \tilde{N} \rangle|^2 = \begin{cases} 0 \\ \frac{|2\lambda_N(-\lambda H_1 H_2 + \kappa S^2)^* + 2\lambda_N A_{\lambda_N} S| - m_{R\bar{R}}^2}{2|\lambda_N|^2} \quad (\text{if } > 0) \end{cases} . \tag{2.19}$$

If $2|m_{R\bar{R}}^2| - m_{R\bar{R}}^2 < 0$, then, a non vanishing VEV is absent and the origin $\tilde{N} = 0$ is the true minimum and vacuum. Of course, this condition is exactly same as the condition for the positiveness of the mass squared of the lighter right-handed sneutrino in Eq. (2.14). Then, the scalar potential is reduced to the Higgs potential in the NMSSM.

As stated in Introduction, the domain wall problem in this simplest Higgs potential can be solved by some modifications [33, 34], which have no impact on the sneutrino physics we are interested in.

2.4 Higgs and neutralino sectors

The inclusion of the S superfield implies two new Higgs states, one CP-even and one CP-odd, which mix with the MSSM Higgs states. We assume that there is no CP-violation in the Higgs sector and therefore CP-even and CP-odd states do not mix. Thus the corresponding mass matrices, which have exactly the same expressions as in the NMSSM, can be written in the respective basis, and the mass eigenstates expressed as a linear superposition of the corresponding gauge eigenstates. For CP-even and CP-odd Higgses, we have

$$H_i^0 = S_{H_i^0}^1 H_{uR}^0 + S_{H_i^0}^2 H_{dR}^0 + S_{H_i^0}^3 S_R, \tag{2.20}$$

and

$$A_a^0 = P_{A_a^0}^1 H_{uI}^0 + P_{A_a^0}^2 H_{dI}^0 + P_{A_a^0}^3 S_I, \tag{2.21}$$

for $i = 1, 2, 3$, $a = 1, 2$, and where the subscripts R and I denote the real and imaginary components of the corresponding fields, respectively. The minimisation of the scalar potential and subsequent calculation of the Higgs masses is carried out with the code `NMHDECAY 2.0` code [41].

The superpartner of the singlet Higgs, the singlino \tilde{S} , has the same quantum numbers as the bino, wino and Higgsinos and therefore mixes with them, giving rise to a fifth neutralino state. This is exactly the same situation as in the NMSSM [34, 36, 30] and the neutralino mass matrix has the same expression. The mass matrix is diagonalized as usual by an unitary matrix $N^{\tilde{\chi}}$. The neutralino mass eigenstates are therefore a linear superposition of bino, wino, Higgsinos and singlino which we express as

$$\tilde{\chi}_i^0 = N_{\tilde{\chi}_i}^1 \tilde{B} + N_{\tilde{\chi}_i}^2 \tilde{W}^3 + N_{\tilde{\chi}_i}^3 \tilde{H}_1^0 + N_{\tilde{\chi}_i}^4 \tilde{H}_2^0 + N_{\tilde{\chi}_i}^5 \tilde{S}. \quad (2.22)$$

2.5 Right-handed sneutrino LSP

The phenomenology of this construction is largely dependent on which particle plays the role of the lightest supersymmetric particle. In the ordinary NMSSM the neutralino is the LSP in extensive regions of the parameter space, thereby providing an interesting candidate for dark matter, which can reproduce the correct relic abundance and be within the sensitivity of some of the future direct detection experiments [30].

In this extended model another possibility arises, since the right-handed sneutrino might also be the LSP. The mass of the lightest right-handed sneutrino, is given by $m_{R\bar{R}}^2 - 2|m_{RR}^2|$ (2.13), and is therefore dependent on the set of new parameters. In particular, as we have shown in Fig. 2, below a certain value of λ_N it is always possible to choose a value of the soft mass parameter, $m_{\tilde{N}}$, for which the right-handed sneutrino mass will be small enough so as to guarantee that it becomes the LSP. Being a neutral particle with electroweak scale interactions, the right-handed sneutrino would therefore constitute a dark matter candidate within the category of WIMPs. We will explore this possibility by analyzing the sneutrino relic abundance and direct detection cross section in the following Sections.

3 Thermal relic density

A crucial feature of this scenario is the existence of direct couplings of the right-handed sneutrino to Higgses and neutralinos. These emerge through the term $\lambda_N S N N$ in the

superpotential (2.2), since as we stated above, the singlet and singlino components of S mix with the CP-even Higgs bosons and neutralinos, respectively. The strength of the interaction is therefore dependent on the value of λ_N and A_{λ_N} . This provides tree-level interactions with ordinary matter which are specified in Appendix A. For adequate values of λ_N (and A_{λ_N}), these couplings would be of electroweak scale, thereby making the right-handed sneutrino a potential WIMP candidate⁴. Still, in order to determine whether or not the right-handed sneutrino is a viable WIMP, its relic density has to be evaluated and compared with the recent measurement by the WMAP satellite, $0.1037 \leq \Omega h^2 \leq 0.1161$. [37].

The possible annihilation products for right-handed sneutrinos in this construction include the following channels

- (i) $W^+ W^-$, $Z Z$, and $f \bar{f}$ via s -channel Higgs exchange;
- (ii) $H_i^0 H_j^0$, via s -channel Higgs exchange, t - and u -channel sneutrino exchange, and a scalar quartic coupling;
- (iii) $A_a^0 A_b^0$, and $H_i^+ H_j^-$, via s -channel Higgs exchange, and a scalar quartic coupling;
- (iv) $Z A_a^0$ and $W^\pm H^\mp$ via s -channel Higgs exchange;
- (v) NN , via s -channel Higgs exchange and via t - and u -channel neutralinos exchange.

The processes suppressed by the neutrino Yukawa y_N (such as s -channel sneutrino annihilation mediated by the Z boson) have not been included, since these are negligible as shown in the previous section. The corresponding expressions for the amplitudes of each channel are listed in Appendix B.

Since all the above annihilations involve s -channel Higgs exchange processes, resonant sneutrino annihilation will take place near the pole, where $m_{\tilde{N}_1} \approx 2m_{H_i^0}$. This implies that the partial-wave expansion method is not sufficiently accurate. Thus, we integrate it directly, following the same procedure detailed in Ref. [38] for the case of the neutralino. In our calculation, we assume the absence of a degenerate particle and do not include possible associated co-annihilation effects. Notice that this could in principle happen between the real and imaginary component of sneutrinos and between the lightest sneutrino and the lightest neutralino. The former situation only arises if

⁴This is contrary to the case of right-handed sneutrinos with the MSSM, which do not present (unsuppressed) tree-level couplings to ordinary matter and therefore have to be generated via non-thermal processes (e.g., late decays of the NLSP) [15, 16, 17, 18].

m_{RR}^2 in (2.14) is very small, which implies some accidental cancellation in (2.13) and only occurs for specific choices of input parameters which we will explicitly avoid. The latter case would only be relevant near those regions in which the sneutrino mass is close to the NLSP mass. These regions of the parameter space can be easily identified and we will comment on this later.

As we explained above, and is evidenced in the different annihilation channels previously detailed, the main feature of this construction is the direct coupling of the sneutrino to the Higgs fields. Hence, the sneutrino annihilation cross section is extremely dependent on the structure of the Higgs sector. Although this introduces a strong dependence of our results on the NMSSM parameter space, there are some general features which are easy to identify and understand.

- The coupling λ_N determines the overall scale of the annihilation cross section. A larger λ_N implies more effective sneutrino annihilation, and in turn a smaller relic abundance, and viceversa. Regarding the supersymmetric spectrum, notice that λ_N only affects the right-handed neutrino and sneutrino masses and does not alter the rest of the NMSSM spectrum. Thus, having chosen a set of viable NMSSM input parameters, the value of λ_N (as well as $m_{\tilde{N}}$ and A_{λ_N}) can be freely varied in order to reproduce the correct sneutrino relic abundance, being only constrained by perturbativity (we will impose $\lambda_N < 1$), the occurrence of tachyons in the sneutrino sector or the upper bound on the sneutrino mass in order for it to be the LSP.
- Annihilation into $H_i^0 H_j^0$ and $A_a^0 A_b^0$ will turn out to be among the most effective channels, as we will later see. Whether these are kinematically allowed or not depends on the Higgs masses. Interestingly, within the framework of the NMSSM, very light CP-even and CP-odd Higgses are possible (as long as they have a significant singlet component), making these channels available for a wide range of sneutrino masses. In the next Section we will show how this can, for instance, make it possible for light sneutrinos to reproduce the correct relic abundance.
- Another relevant contribution to the total annihilation cross section is due to the annihilation into a pair of right-handed neutrinos, N . This channel is kinematically allowed when $m_{\tilde{N}_1} > M_N$. As we saw in Fig. 1, this is allowed above a certain value of the soft sneutrino mass, $m_{\tilde{N}}$, which depends on the specific values of λ_N and A_{λ_N} and which increases for larger λ_N .

- Finally, for all the possible annihilation products there is always a contribution coming from s -channel CP-even Higgs exchange. This implies that all of them are subject to a resonant effect when $2m_{\tilde{N}_1} \approx m_{H_i^0}$, for $i = 1, 2, 3$. The occurrence of resonant sneutrino annihilation gives rise to a characteristic decrease of the relic abundance at the corresponding values of the sneutrino mass. Furthermore, given the possibility of light scalar Higgses in the NMSSM, this resonant annihilation can be present even for light sneutrinos.

Having understood the basic properties of right-handed sneutrino annihilation in this framework, we will now proceed to explore the parameter space and provide specific examples which show how the correct thermal relic abundance can be obtained.

3.1 Numerical examples

The input parameters of this scenario are, on the one hand, the usual NMSSM parameters, which we define at low-energy,

$$\lambda, \kappa, \tan\beta, \mu, A_\lambda, A_\kappa. \quad (3.23)$$

The soft supersymmetry-breaking terms, namely gaugino masses, $M_{1,2,3}$, flavour independent scalar masses, $m_{Q,L,U,D,E}$, and trilinear parameters, $A_{U,D,E}$, are also taken as free parameters and specified at low scale. More specifically, we have assumed they mimic, at low-energy the values obtained from a hypothetical GUT unification. Thus we set $M_1 : M_2 : M_3 = 1 : 2 : 6$. The present lower bound on a possible supersymmetric contribution to the muon anomalous magnetic moment, sets stringent upper constraints on the mass of sleptons. As it was shown in [30], for small values of $\tan\beta$ the experimental result can be reproduced with the choice $m_{L,E} = 150$ GeV and $A_E = -2500$ GeV and a small value for the gaugino mass⁵, $M_1 \lesssim 160$ GeV. Larger values of $\tan\beta$ are, however less constrained [39]. In order to satisfy the experimental constraint on the branching ratio of the $b \rightarrow s\gamma$ rare decay a careful choice has to be made of parameters in (3.23). More details on the conditions under which these bounds can be fulfilled can be found in [30, 40].

⁵It should be stressed that if one does not wish to impose the bound on the muon anomalous magnetic moment (motivated e.g. by tau data, which lead to a better agreement with the SM result), large slepton masses, equal to squark masses can be chose. This would, however, have no consequence on the calculation of neither the relic abundance of right-handed sneutrinos, nor in their detection cross section.

The analysis of the low-energy NMSSM phenomenology has been performed with the `NMHDECAY 2.0` code [41], which minimises the scalar potential, dismissing the presence of tachyons and/or false minima, and computes the Higgs boson masses including 1- and 2-loop radiative corrections, as well as the rest of the supersymmetric masses. Based on this code, we have built a set of routines which numerically calculate the right-handed sneutrino spectrum and relic density as described in the previous section.

More specifically, we impose the experimental bound on the branching ratio of the rare $b \rightarrow s\gamma$ decay, $2.85 \times 10^{-4} \leq \text{BR}(b \rightarrow s\gamma) \leq 4.25 \times 10^{-4}$ at 2σ level, obtained from the experimental world average reported by the Heavy Flavour Averaging Group [44], and the theoretical calculation in the Standard Model [45], with errors combined in quadrature. We also take into account the upper constraint on the $B_S \rightarrow \mu^+\mu^-$ branching ratio obtained by CDF, $\text{BR}(B_S \rightarrow \mu^+\mu^-) < 5.8 \times 10^{-8}$ at 95% c.l. [42] (which improves the previous one from D0 [43]).

Regarding the muon anomalous magnetic moment, a constraint on the supersymmetric contribution to this observable, a_μ^{SUSY} , can be extracted by comparing the experimental result [46], with the most recent theoretical evaluations of the Standard Model contributions [47, 48, 49]. When e^+e^- data are used the experimental excess in $a_\mu \equiv (g_\mu - 2)/2$ would constrain a possible supersymmetric contribution to be $a_\mu^{\text{SUSY}} = (27.6 \pm 8) \times 10^{-10}$, where theoretical and experimental errors have been combined in quadrature. However, when tau data are used, a smaller discrepancy with the experimental measurement is found. Due to this reason, in our analysis we will not impose this constraint, but only indicate whether the points are compatible with it at the 2σ level, for which we assume the range $11.6 \times 10^{-10} \leq a_\mu^{\text{SUSY}} \leq 43.6 \times 10^{-10}$.

The inclusion of the new superfield N and the corresponding terms in the superpotential and Lagrangian leaves three new parameters to be fixed. Following the discussion in the previous section, these can be chosen as

$$\lambda_N, m_{\tilde{N}}, A_{\lambda_N}. \quad (3.24)$$

These, together with the NMSSM parameters (3.23) fully specify the model. Our task is now to determine whether the correct sneutrino relic density can be obtained with reasonable choices of the above set of parameters.

Let us now illustrate with some examples the theoretical predictions for the relic abundance of right-handed sneutrinos and the various possibilities which allow to reproduce the correct relic density. The sets of parameters for each example are detailed

	A)	B1)	B2)	C)
$\tan \beta$	5	5	5	3.5
A_λ	550 GeV	400 GeV	400 GeV	480 GeV
A_κ	-200 GeV	0 GeV	0 GeV	-50 GeV
μ	130 GeV	200 GeV	200 GeV	230 GeV
(λ, κ)	(0.2, 0.1)	(0.1, 0.05)	(0.3, 0.2)	(0.5, 0.3)
M_1	200 GeV	150 GeV	150 GeV	300 GeV
$m_{L,E}$	250 GeV	250 GeV	250 GeV	250 GeV
$m_{Q,U,D}$	1000 GeV	1000 GeV	1000 GeV	1000 GeV
A_E	-2500 GeV	-2500 GeV	-2500 GeV	-2500 GeV
$A_{U,D}$	1500 GeV	1500 GeV	1500 GeV	1000 GeV
$m_{H_1^0}$	62.4 GeV	117.7 GeV	116.2 GeV	115.1 GeV
$m_{H_2^0}$	119.4 GeV	200.8 GeV	267.7 GeV	263.5 GeV
$m_{H_3^0}$	634.1 GeV	706.4 GeV	730.6 GeV	725.4 GeV
$m_{A_1^0}$	199.6 GeV	14.2 GeV	47.6 GeV	169.7 GeV
$m_{A_2^0}$	632.5 GeV	705.1 GeV	727.9 GeV	719.5 GeV
$m_{\tilde{\chi}_1^0}$	95.8 GeV	126.3 GeV	124.3 GeV	190.1 GeV
$\text{BR}(b \rightarrow s\gamma)$	4.15×10^{-4}	4.02×10^{-4}	4.02×10^{-4}	4.03×10^{-4}
a_μ^{SUSY}	4.08×10^{-10}	5.58×10^{-10}	8.05×10^{-10}	2.96×10^{-10}

Table 1: Set of inputs corresponding to the examples used in the analysis, together with the predicted values of $\text{BR}(b \rightarrow s\gamma)$ and a_μ^{SUSY} and the relevant part of the resulting supersymmetric spectrum.

in Table 1, together with the predicted values⁶ of $\text{BR}(b \rightarrow s\gamma)$ and a_μ^{SUSY} .

3.1.1 Predominant annihilation into scalar Higgses

As already mentioned, sneutrino annihilations into Higgs bosons are generally among the dominant channels, when they are kinematically allowed. This is also the case in other models for thermal right-handed sneutrino [23]. However, in our case, the flexibility and interesting properties of the Higgs sector of the NMSSM make this possibility much very versatile.

As an specific example we will choose the NMSSM input parameters as in case A) of Table 1. This point is very characteristic of the NMSSM since light CP-even Higgses are possible. In this case the lightest Higgs has a mass $m_{H_1^0} \approx 62$ GeV, which is consistent with the present LEP constraints due to its large singlet component ($(S_{H_1^0}^3)^2 = 0.997$). The second lightest Higgs is MSSM-like and has a mass of $m_{H_2^0} \approx 120$ GeV. The lightest neutralino is a mixed bino-Higgsino-singlino state ($(N_{\tilde{\chi}_1^1}^1)^2 \approx 0.1$, $(N_{\tilde{\chi}_1^1}^3)^2 + (N_{\tilde{\chi}_1^1}^4)^2 \approx 0.7$ and $(N_{\tilde{\chi}_1^1}^5)^2 \approx 0.2$). Its mass is $m_{\tilde{\chi}_1^0} \approx 96$ GeV, and this sets the upper bound for the sneutrino mass if the latter is to be the LSP. Regarding the right-handed sneutrino sector, its mass is a function of the parameters λ_N , $m_{\tilde{N}}$ and A_{λ_N} , as explained in the previous section. As a first example we have fixed $A_{\lambda_N} = -250$ GeV and performed a scan in the allowed range for the λ_N , $m_{\tilde{N}}$ parameters.

The resulting sneutrino annihilation cross section is shown in Fig. 4, together with the contribution for each individual channel, as a function of the sneutrino mass for $\lambda_N = 0.06$ (the variation in the sneutrino mass is achieved with a scan in $m_{\tilde{N}}$). A first thing to notice is that the various annihilation channels display a resonant enhancement due to the two lightest CP-even Higgses when the sneutrino mass is approximately one half of the Higgs mass for the two lightest scalar Higgses, i.e., $m_{\tilde{N}_1} \approx 30$ GeV and 60 GeV. The resonance due to the third scalar Higgs state is not observed since it would occur for large masses ($m_{\tilde{N}_1} \approx 317$ GeV), for which the right-handed sneutrino is no longer the LSP.

In this example, annihilation into a pair of lightest CP-even Higgses dominates the total annihilation cross section once this channel becomes kinematically allowed (for $m_{\tilde{N}_1} > m_{H_1^0} \approx 62$ GeV). Lighter sneutrinos can only annihilate into a pair fermion-

⁶Some of these examples are inspired in the scenarios analysed in [30] (e.g., cases B1) and B2) are similar to the case studied in Fig. 7 there), and we refer the reader to that work for a more detailed study of the NMSSM parameter space and associated experimental constraints.

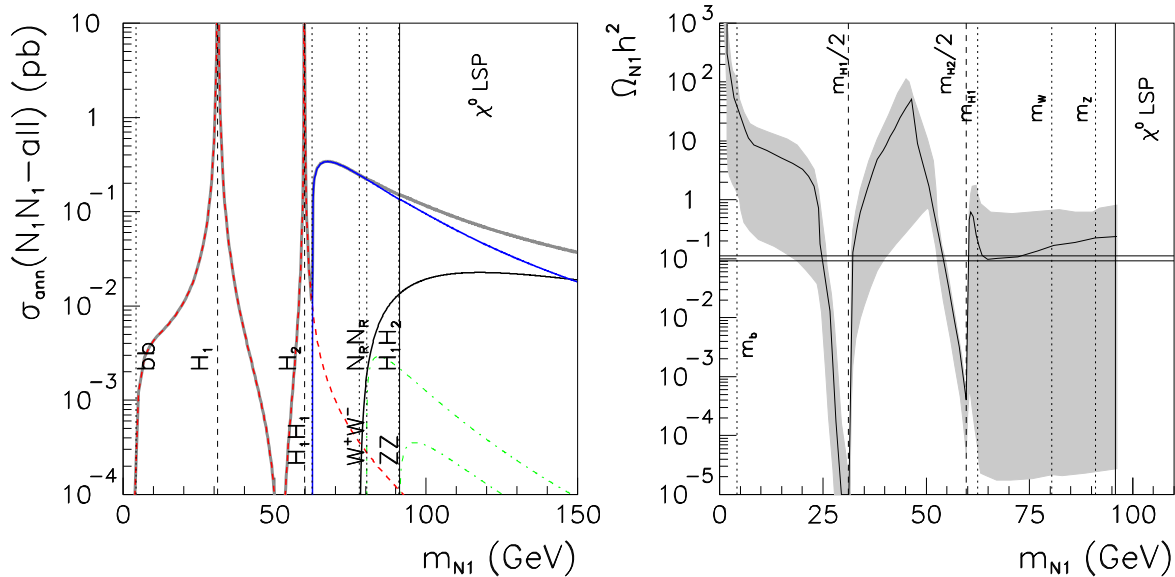


Figure 4: Left) Total sneutrino annihilation cross-section as a function of the sneutrino mass (grey thick solid line) for example A) of Table.1 with $(\lambda, \kappa) = (0.2, 0.1)$, and $\lambda_N = 0.06$. The contributions from the different annihilation channels are indicated as follows, dashed red line for $f\bar{f}$, dot-dashed green lines for ZZ and W^+W^- , solid blue line for $H_i^0 H_j^0$, and solid black line for NN . Vertical dashed lines indicate the location of the resonances in the s -channels when $2m_{\tilde{N}_1} \approx m_{H_i^0}$, whereas vertical dotted lines indicate when the different annihilation channels become kinematically accessible. The vertical solid line indicates the point at which the neutralino becomes the LSP. Right) Theoretical predictions for the sneutrino relic density as a function of the sneutrino mass for the same example, but for a scan with $\lambda_N \in [0.05, 0.1]$ and $m_{\tilde{N}} \in [0, 150]$ GeV. The solid line indicates the result for $\lambda_N = 0.06$.

antifermion, being $b\bar{b}$ the leading contribution. As observed in the plot, for this choice of parameters this channel is less effective and only provides a sufficiently large annihilation cross section close to the resonances of the scalar Higgses⁷. Notice also that although annihilation into a pair of right-handed neutrinos is also possible for sneutrinos heavier than 80 GeV, this channel only becomes comparable to the Higgs contribution for sneutrino masses of order 150 GeV, for which the sneutrino is no longer the LSP.

The resulting theoretical predictions for the relic density are depicted on the right

⁷We remind the reader that for a WIMP of mass 100 GeV the necessary annihilation cross-section in order to reproduce the WMAP result is around $\sigma_{ann} \sim 0.1$ pb.

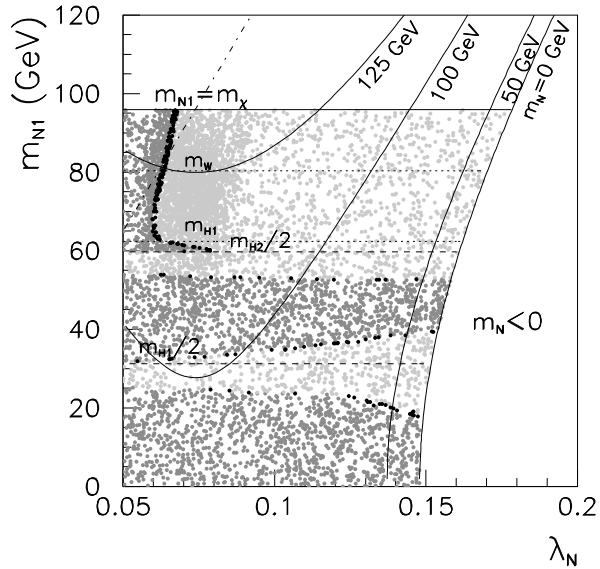


Figure 5: Effect of the relic density constraint on the $(\lambda_N, m_{\tilde{N}_1})$ plane for case A) in Table 1 with $A_{\lambda_N} = -250$ GeV. Black dots represent the regions where the sneutrino relic abundance is in agreement with the WMAP constraint, whereas light(dark) grey dots represent those where the sneutrino relic abundance is smaller(larger). The curved solid lines indicate the trajectories with a fixed value of the sneutrino soft mass $m_{\tilde{N}}$.

hand-side of Fig. 4 for a scan of λ_N in the range $\lambda_N \in [0.05, 0.1]$ and a scan in the allowed values for $m_{\tilde{N}}$. The solid line indicates the result for $\lambda_N = 0.06$. We can see how light sneutrinos with masses as small as approximately 25 GeV can be obtained with the correct relic abundance due to the resonant effects in the Higgs diagrams. Once annihilation into scalar Higgses is allowed, the correct relic abundance can be obtained in the whole range⁸ $m_{\tilde{N}_1} \approx 60 - 90$ GeV with $\lambda_N \approx 0.06$.

For a better understanding of the effect of the relic density constraint on the sneutrino parameters, we represent in Fig. 5 the $(\lambda_N, m_{\tilde{N}_1})$ plane, indicating with black dots the regions where the sneutrino relic abundance is in agreement with the WMAP result. Dark grey dots represent the areas in which the sneutrino relic abundance exceeds the WMAP constraint and light grey dots are those in which the sneutrino relic density is smaller than the WMAP bound. The contours for a fixed sneutrino soft mass, $m_{\tilde{N}}$, are indicated by means of solid lines. As already explained, when annihilation into a pair of Higgs bosons is allowed, a value of $\lambda_N \approx 0.06$ is favoured in this example. As we

⁸Since co-annihilation effects have not been included, our result for the relic abundance is not exact when $m_{\tilde{N}_1} \approx m_{\tilde{\chi}_1^0}$.

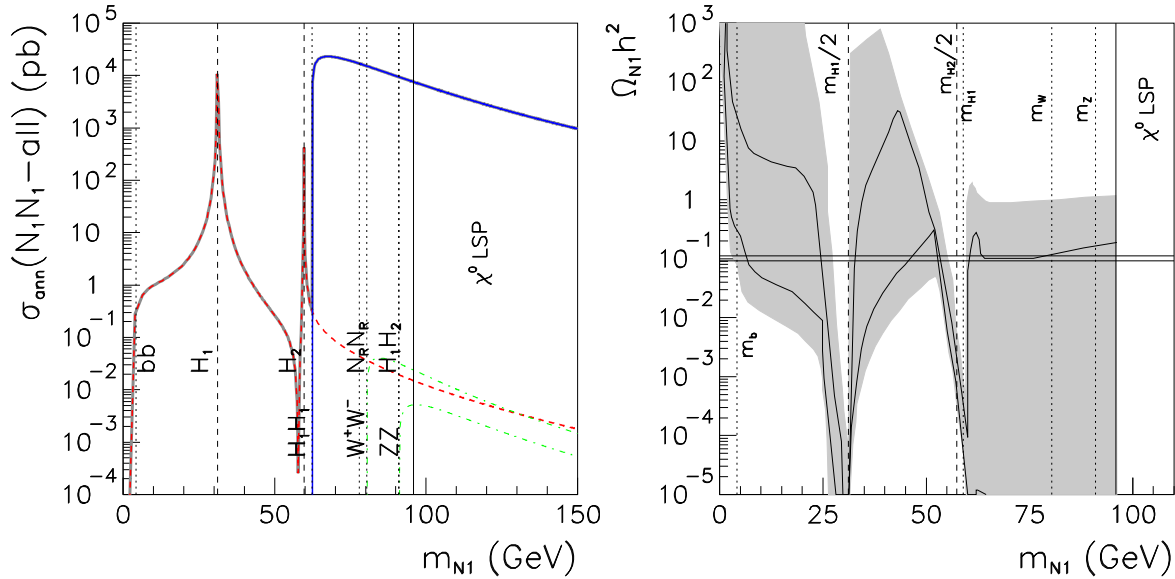


Figure 6: Left) The same as in Fig.7 (case A) in Table 1) but with $A_{\lambda_N} = -500$ GeV and $\lambda_N = 0.25$. Right) Theoretical predictions for the sneutrino relic density as a function of the sneutrino mass for the same example, but for a scan with $\lambda_N \in [0.05, 0.35]$ and $m_{\tilde{N}} \in [0, 250]$ GeV. The solid lines indicate, from top to bottom, the result for $\lambda_N = 0.11, 0.25$.

see, this corresponds to values of the sneutrino soft mass in the range 100 – 150 GeV. Otherwise the relic density is too large except along the resonances (the fine-tuned near horizontal strips), for which the value of λ_N can be as large as 0.15.

3.1.2 Predominant annihilation into $b\bar{b}$ and very light sneutrinos

Obtaining the correct relic density with only annihilation into $b\bar{b}$ would require a larger value of λ_N . However, as we can see from Fig. 5, if we restrict ourselves to positive values of $m_{\tilde{N}}$ then for this choice of parameters there is an upper bound $\lambda_N \lesssim 0.15 - 0.18$. Remember however from the previous section that an increase in $|A_{\lambda_N}|$ allows larger values of λ_N . With this in mind, we have reanalysed the previous example, case A) in Table 1, but now using $A_{\lambda_N} = -500$ GeV, for which values of λ_N up to 0.35 can be used. This considerably increases the annihilation cross section.

For this example, Fig. 6 represents the annihilation cross section for $\lambda_N = 0.25$ and a scan in the allowed values of $m_{\tilde{N}}$. The $b\bar{b}$ contribution is now significantly larger, reaching values of order of 1 pb without the need of resonant effects. Similarly, the Higgs

contribution also increases considerably, thereby leading to a too large annihilation cross section (notice the different scale on the plot). On the right-hand side of Fig. 6 the resulting sneutrino relic abundance is plotted for a scan with $\lambda_N \in [0.05, 0.35]$ and $m_{\tilde{N}} \in [0, 250]$ GeV, where the solid lines indicate, from top to bottom, the particular cases $\lambda_N = 0.11$ (which yields similar results as the example studied in Section 3.1.1) and 0.25. Interestingly, as we can see, for such large values of λ_N light sneutrinos with masses $m_{\tilde{N}_1} \gtrsim 5$ GeV can reproduce the correct relic abundance.

3.1.3 Predominant annihilation into pseudoscalar Higgses

Another interesting possibility is sneutrino annihilation into a pair of pseudoscalar Higgses. Although the pseudoscalar is rather heavy in the MSSM (and experimentally constrained to be above 93.4 GeV [62]), in the NMSSM (where an extra CP-odd state is present) it can be much lighter in some regions of the parameter space and experimentally allowed if it has a large singlet component [63, 64, 65]. This therefore implies that this channel can be kinematically allowed for lighter sneutrinos.

In order to illustrate this possibility, we have taken the NMSSM input parameters as indicated in example B1) of Table 1. This point in the NMSSM parameter space is a good example of how light pseudoscalars might be phenomenologically viable. In this case the lightest pseudoscalar has a mass $m_{A_1^0} = 14.2$ GeV and it is singlet-like. The lightest scalar Higgs is MSSM-like with a mass $m_{H_1^0} \approx 116$ GeV, whereas the second lightest Higgs, with $m_{H_2^0} \approx 200$ GeV is mostly singlet. The lightest neutralino is a mixed bino-Higgsino state ($(N_{\tilde{\chi}_1^1}^1)^2 \approx 0.66$ and $(N_{\tilde{\chi}_1^1}^3)^2 + (N_{\tilde{\chi}_1^1}^4)^2 \approx 0.25$) with a mass $m_{\tilde{\chi}_1^0} = 126$ GeV. It would be the lightest supersymmetric particle in the NMSSM for this choice of parameters and therefore sets once more the upper limit for allowed values of the right-handed sneutrino mass. Regarding the right-handed sneutrino sector, we have fixed $A_{\lambda_N} = -500$ GeV and performed a scan in the $\lambda_N, m_{\tilde{N}}$ parameters. This is precisely the same example that was displayed on Fig. 2. As one can extract from there, a maximal value of $\lambda_N \sim 0.11$ can be used, with the soft sneutrino mass ranging from $m_{\tilde{N}} = 0$ to approximately $m_{\tilde{N}} = 235$ GeV.

The predicted sneutrino annihilation cross section is represented on the left hand-side of Fig. 7 as a function of the sneutrino mass, together with the contributions from each individual annihilation channel. As we can see, for this example the annihilation into a pair of CP-odd Higgses largely dominates over the other contributions. This is particularly true for light sneutrinos since, due to the smallness of $m_{A_1^0}$, this channel

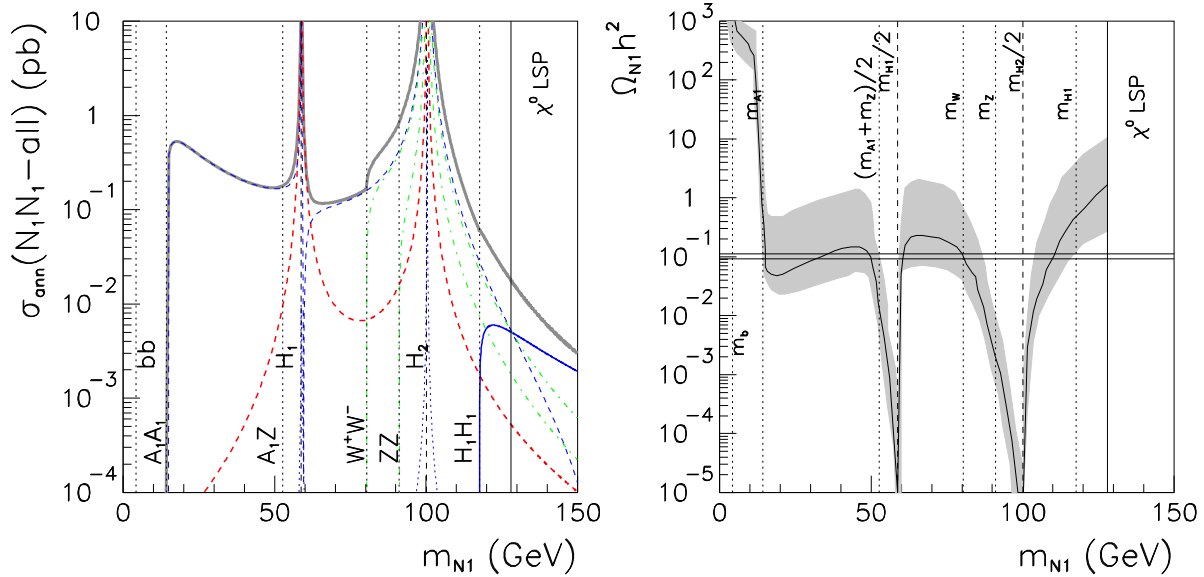


Figure 7: Left) The same as in Fig. 4 but for example B1) of Table,1 with $\lambda = 0.1$, $\kappa = 0.05$, and $\lambda_N = 0.07$. Here the dashed blue line denotes the contribution of the $A_a^0 A_b^0$ channel and the dotted blue line (only visible in the Higgs resonances) the contribution of $A_a^0 Z$. Right) Theoretical predictions for the sneutrino relic density as a function of the sneutrino mass for the same example, but for a scan with $\lambda_N \in [0.05, 0.1]$ and $m_{\tilde{N}} \in [0, 250]$ GeV. The solid line indicates the result for $\lambda_N = 0.07$.

is kinematically available for $m_{\tilde{N}_1} \gtrsim 14$ GeV. Note that for lighter sneutrinos the only possibility is annihilation into a pair of $f\bar{f}$, which is less effective. The abrupt enhancements at the resonances of the Higgs-exchanging s -channels when $2m_{\tilde{N}_1} \sim m_{H_1^0}, m_{H_2^0}$ are also observed for every channel at $m_{\tilde{N}_1} \approx 58$ GeV and 100 GeV.

The theoretical predictions for the resulting relic density are depicted on the right hand-side of Fig. 7 for the range $\lambda_N \in [0.05, 0.11]$. As we see there, the correct relic density can be obtained for a wide range of sneutrino masses. In particular, sneutrinos as light as $m_{\tilde{N}_1} \approx 15$ GeV are now possible due to their very effective annihilation into a pair of CP-odd Higgses. This is particularly interesting, since these light sneutrinos have different properties from those obtained in case A). In case A) they could only annihilate into $b\bar{b}$ and thus the coupling λ_N had to be of order 0.25. However, in the present case the coupling can be much smaller and $\lambda_N \approx 0.07$ suffices to obtain the correct relic abundance. This will have very interesting properties for their detection, as we will see in Section 4.

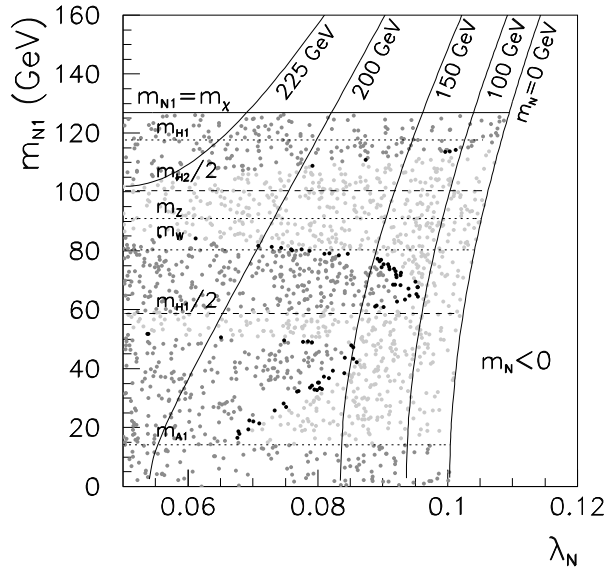


Figure 8: The same as in Fig. 5 but for case B1) of Table 1 with $A_{\lambda_N} = -500$ GeV.

The effect of the relic density constraint on the $(\lambda_N, m_{\tilde{N}_1})$ plane is shown in Fig. 8, together with the contours for a fixed sneutrino soft mass, $m_{\tilde{N}}$. As we observe, values of the sneutrino coupling constant to the Higgs of order $\lambda_N \approx 0.06 - 0.1$ are sufficient to have viable sneutrino dark matter, whereas values of the soft sneutrino mass around $m_{\tilde{N}} \approx 100 - 200$ GeV seem to be preferred. Once more, along the Higgs resonances sneutrino annihilation is more effective and smaller values of λ_N are needed to obtain the correct abundance. Remarkably, the region corresponding to viable very light sneutrinos (with masses in the 15 – 40 GeV range) can be obtained without requiring a fine-tuning in the λ_N or $m_{\tilde{N}}$ parameters⁹.

The sneutrino properties are extremely sensitive to the NMSSM Higgs sector. One should therefore expect that the above analysis and preferred values for the sneutrino parameters could vary for a different set of NMSSM inputs. In particular, given a different point of the (λ, κ) plane and due to the changes in the (scalar and pseudoscalar) Higgs masses and mixings, the values of the sneutrino mass at which the various channels open and the conditions for resonant annihilation would differ.

This is indeed the case. For instance, for the same choice of parameters as in

⁹Remember, however that there is a certain fine tuning in the NMSSM parameters in order to obtain very light viable pseudoscalars. Still, very light right-handed sneutrinos in this construction are much more natural than very light neutralinos in the NMSSM, for which the extra condition of a resonant annihilation with the very light CP-even Higgs, $2m_{\tilde{\chi}_1^0} \approx m_{A^0}$ is necessary [64].

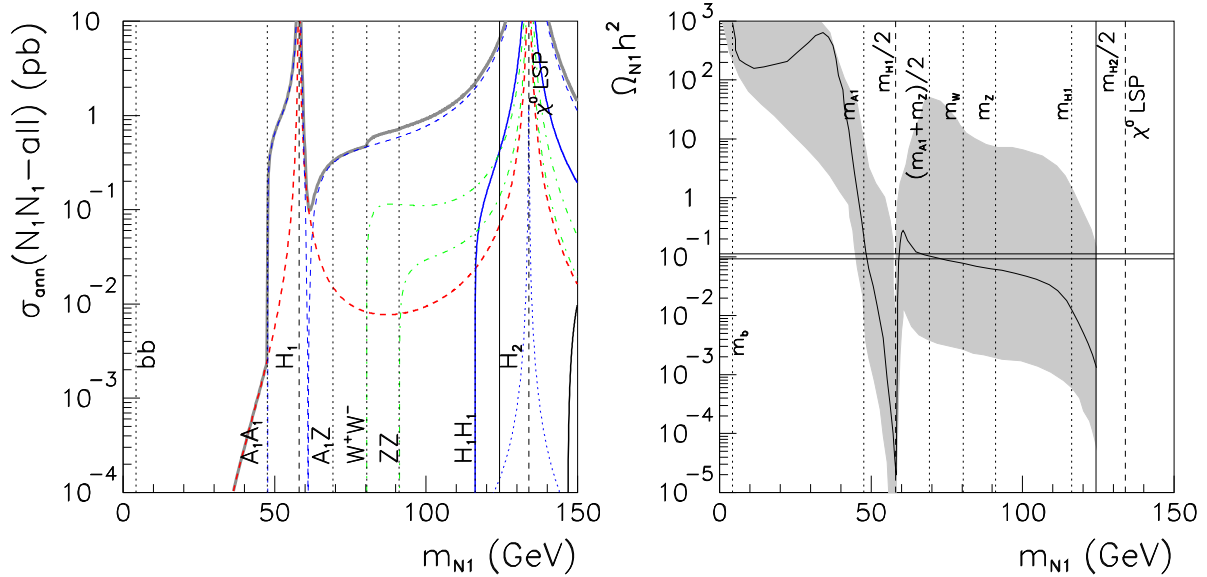


Figure 9: Left) The same as in Fig.7 but for case B2) of Table 1 with $\lambda_N = 0.14$. Right) Corresponding relic density as a function of the sneutrino mass for $\lambda_N \in [0.05, 0.35]$. The solid line indicates the result for $\lambda_N = 0.14$.

example the previous example, let us now choose $(\lambda, \kappa) = (0.3, 0.2)$, corresponding to case B2) in Table 1. This implies an increase of the pseudoscalar mass (and a mild reduction of its singlet component) for which $m_{A_1^0} \approx 48$ GeV, as well as an increase in the mass of the second lightest scalar Higgs, which remains being singlet-like (the lightest scalar Higgs is still MSSM-like and has a mass $m_{H_1^0} \approx 116$ GeV). The rest of the spectrum is detailed in Table 1.

As a consequence of these changes, annihilation into pseudoscalars is no longer possible for very light sneutrinos, which can now only do it into $b\bar{b}$ and their annihilation cross-section becomes much smaller (for the same value of λ_N) than in example A). For sneutrinos with masses above 50 GeV the pseudoscalar channel is still the dominant one, with a modest contribution from annihilation into a pair of gauge bosons when these are kinematically allowed. This can be observed on the left-hand side of Fig. 9, where the corresponding predictions for the sneutrino annihilation cross section are shown for $\lambda_N = 0.14$. Notice also that due to the change in the CP-even Higgs masses, the position of the resonances change, in particular, the resonance due to the second heaviest Higgs is not present (it would occur for $m_{\tilde{N}_1} \approx 200$ GeV, a mass for which the sneutrino is no longer the LSP).

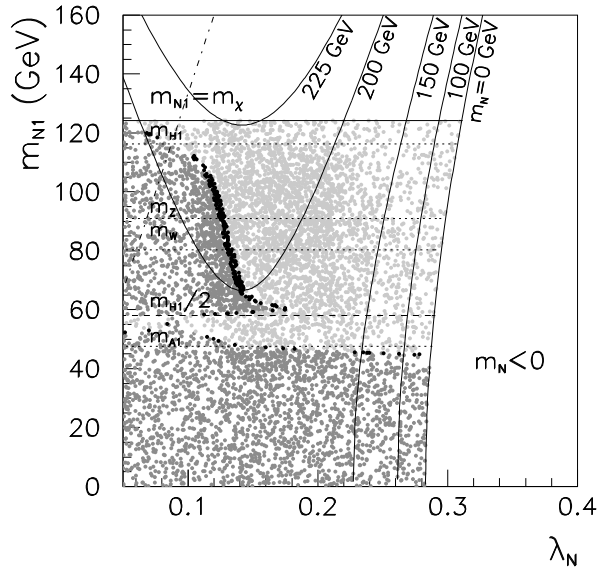


Figure 10: The same as in Fig. 5 but for case B2) of Table 1 with $A_{\lambda_N} = -500$ GeV.

As illustrated on the right-hand side of Fig. 9, the correct relic abundance can still be obtained for a given range of sneutrino masses. As in the previous examples, we perform a scan in the allowed values of λ_N and $m_{\tilde{N}}$ for $A_{\lambda_N} = -500$ GeV. As explained in the previous section, due to the increase in A_{λ_N} , larger values of λ_N are viable.

The effect of the relic density constraint on the $(\lambda_N, m_{\tilde{N}_1})$ plane is displayed in Fig. 10. The allowed areas for sneutrinos heavier than 60 GeV correspond to $\lambda_N \approx 0.12 - 0.14$ with a sneutrino soft mass of order $m_{\tilde{N}} \approx 200 - 225$ GeV, whereas lighter sneutrinos are only viable in the thin region corresponding to resonant annihilation with the lightest scalar Higgs.

As we see from examples B1) and B2), through adequate variations in the sneutrino parameters (3.24), it is possible to find different points in the (λ, κ) plane where the sneutrino has the correct relic density. Variations on the λ and κ parameters have a large impact on the neutralino and Higgs sector and it is therefore not surprising that as a consequence the resulting sneutrino phenomenology is significantly altered. However, the flexibility in the sneutrino properties (especially the freedom in choosing an adequate value of its couplings through λ_N) makes it possible to obtain viable sneutrino dark matter for a wide choice of NMSSM parameters.

In order to illustrate this we have combined a scan in the (λ, κ) plane, in the range $\lambda, \kappa = 0.07 - 0.7$ with a scan in the sneutrino parameters taking $m_{\tilde{N}} = 0 - 250$ GeV

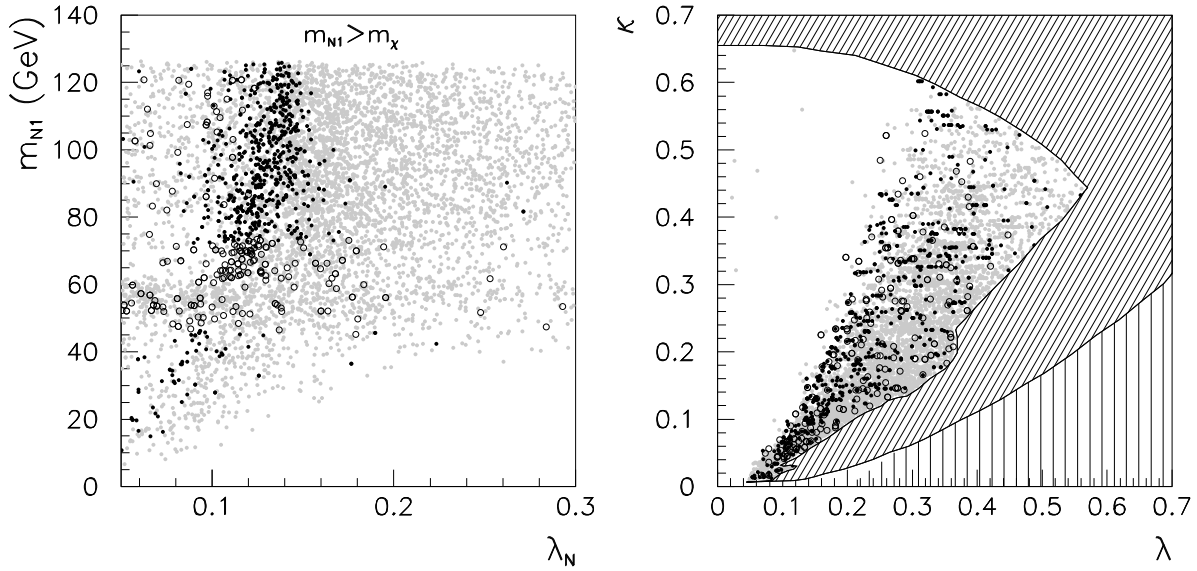


Figure 11: Left) The same as in Fig. 5 but for a scan in (λ, κ) as described in the text. Empty circles correspond to points with the correct relic abundance due to resonant annihilation effects. Right) Regions with the correct sneutrino relic abundance (black dots) in the (λ, κ) plane. The oblique ruled area is excluded due to the occurrence of Landau Poles or because of experimental constraints in the Higgs sector, whereas the vertical ruled area is ruled out due to tachyons in the Higgs sector.

and $\lambda_N = 0.05 - 0.3$. We have fixed $A_{\lambda_N} = -500$ GeV and we have taken otherwise the same NMSSM parameters as in example B1) and B2) of Table 1. On the left-hand side of Fig. 11 we represent the resulting sneutrino mass as a function of the coupling λ_N . Black dots represent those with the correct relic abundance and light points correspond to those where the sneutrino relic density is smaller than the WMAP results (points with a relic density exceeding the WMAP constraint are not shown). As we can see, the correct relic abundance can be obtained within a range of $\lambda_N \approx 0.06 - 0.15$ and for a wide range of sneutrino masses. On the right-hand side of Fig. 11 the regions with the correct relic abundance are displayed on the (λ, κ) plane. We clearly see that the sneutrino can be a viable candidate (for an adequate choice of the λ_N and $m_{\tilde{N}}$ parameters) in virtually any point in this plane. Notice that the absence of points in the left-hand side of the plot is due to the fact that the imaginary component of the sneutrino becomes the lightest one, as explained in Section 2. This is in principle no problem and in fact the imaginary sneutrino would have almost the same properties

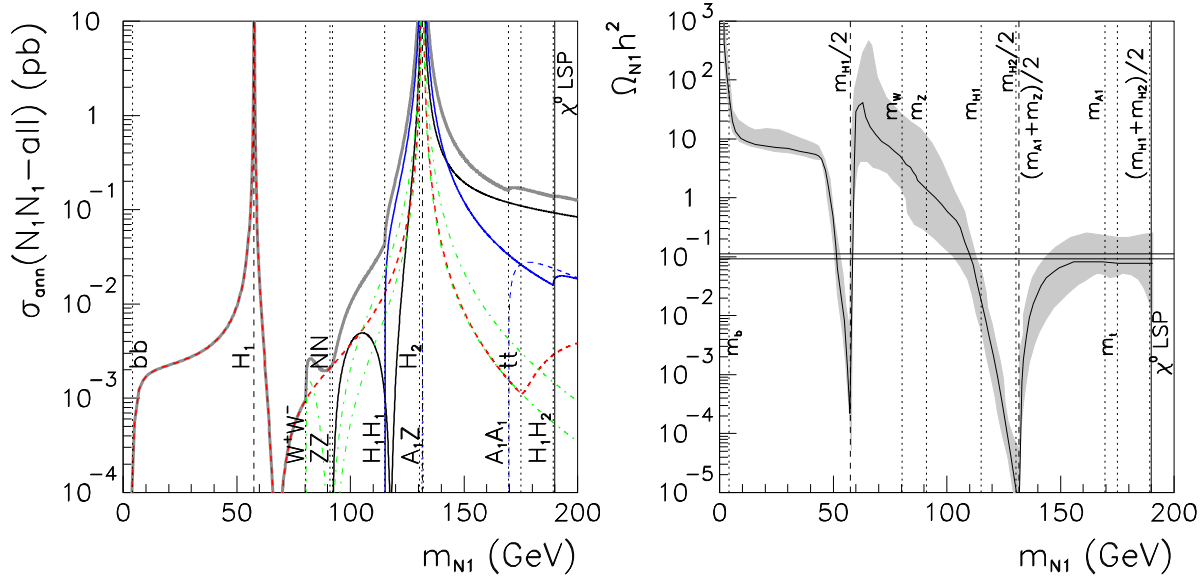


Figure 12: Left) The same as in Fig.7 but for case C) of Table 1 with $\lambda_N = 0.15$ and $A_{\lambda_N} = -250$ GeV. Right) Corresponding relic density as a function of the sneutrino mass for $\lambda_N \in [0.1, 0.3]$. The solid line indicates the result for $\lambda_N = 0.15$.

as the real component¹⁰, however, as we mentioned earlier, for simplicity we have not considered such a possibility here.

3.1.4 Predominant annihilation into right-handed neutrinos or gauge bosons

Let us finally illustrate with another example the relevance of other annihilation channels, in particular the annihilation into a pair of right-handed neutrinos. Our set of input parameters is chosen according to example C) in Table 1, where we also specify the resulting spectrum.

We fix $A_{\lambda_N} = -250$ GeV and plot the resulting annihilation cross section for each individual channel on the left-hand side of Fig. 12. Once more, the features of the Higgs sector clearly affect the calculation of the relic density for the sneutrino. In this example the resonant annihilation through the exchange of the two lightest Higgses is visible at $m_{\tilde{N}_1} \approx 58$ GeV and 130 GeV. The lightest Higgs in this example is doublet-like, whereas the intermediate Higgs, H_2 , and the lightest pseudoscalar are almost

¹⁰The only difference arises in the expression for its annihilation into right-handed neutrinos, as explained in Appendix B.

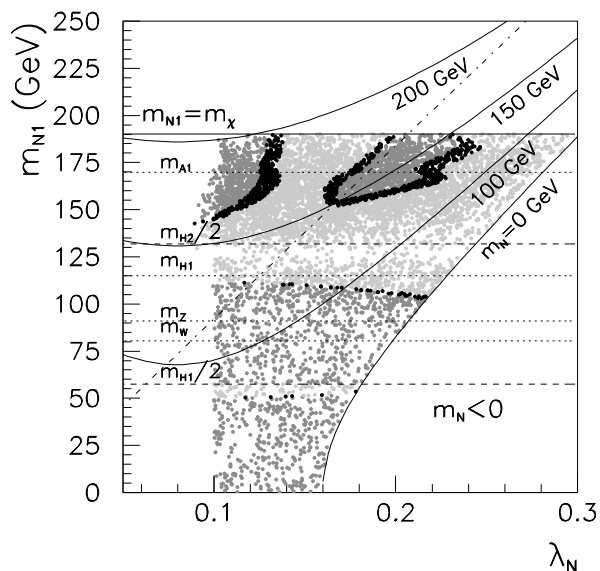


Figure 13: The same as in Fig. 5 but for case C) of Table 1 with $A_{\lambda_N} = -250$ GeV.

pure singlets. Sneutrino annihilation into $b\bar{b}$ is the only possibility for sneutrino masses below M_W , but this channel is only effective when resonant annihilation through the lightest Higgs takes place. Annihilation into ZZ or W^+W^- is the dominant channel below the Higgs production threshold. Interestingly, after the second Higgs resonance, annihilation into a pair of right-handed neutrinos becomes the leading contribution for $m_{\tilde{N}_1} \gtrsim 150$ GeV, although the contributions of the $H_1^0 H_1^0$ and $A_1^0 A_1^0$ channels are not negligible.

The resulting relic density is shown on the right-hand side of Fig. 12 for a scan with $\lambda_N \in [0.1, 0.3]$ and $m_{\tilde{N}} \in [0, 200]$ GeV. The solid line indicates the result for $\lambda_N = 0.15$. We find that in this example the correct relic density can be obtained through annihilation into ZZ or W^+W^- (for sneutrinos with a mass around 100 GeV and $\lambda_N \approx 0.2$) or annihilation into NN and $H_1^0 H_1^0$ for sneutrinos above $m_{\tilde{N}_1} \gtrsim 140$ GeV, in which case $\lambda_N \approx 0.1$ is necessary.

The corresponding $(\lambda_N, m_{\tilde{N}_1})$ plane is shown in Fig. 13, indicating the regions consistent with the WMAP constraint on the relic density. Consistently with the discussion above, in the region above the dot-dashed line (which corresponds to the area in which the sneutrino mass is larger than the right-handed neutrino mass, $m_{\tilde{N}_1} > M_N$) there is a wide region with $\lambda_N \approx 0.1$ for which the WMAP constraint is satisfied. This also corresponds to values of the soft sneutrino masses in the range $m_{\tilde{N}} = 150 - 200$ GeV. Notice also a second region for larger values of λ_N of order $0.15 - 0.18$. Below the

dot-dashed line, where $m_{\tilde{N}_1} < M_N$ the WMAP region corresponds to values of the sneutrino-Higgs coupling in the range $\lambda_N = 0.15 - 0.24$, and smaller values of the sneutrino soft mass, $m_{\tilde{N}} = 100 - 150$ GeV. Light sneutrinos in this example have a too large relic abundance and it is only along the regions with resonant annihilation that the WMAP constraint is satisfied.

3.2 Overview

Throughout this section we have seen how the right-handed sneutrino can reproduce the correct dark matter abundance under different conditions and for various points in the NMSSM parameter space. In this sense, the flexibility to choose adequate values of the sneutrino parameters λ_N , $m_{\tilde{N}}$ and A_{λ_N} was very useful. Notice in any case that the preferred values of these parameters are quite natural. The sneutrino-Higgs coupling λ_N can be chosen in the range $\lambda_N = 0.05 - 0.4$ and the sneutrino soft mass could be of order of $100 - 250$ GeV, being of the same order than the slepton soft masses in our examples. As a result, sneutrinos in the mass range $m_{\tilde{N}_1} \approx 5 - 200$ GeV are found that can reproduce the WMAP constraint on the relic abundance.

It should also be noted that obtaining heavier right-handed sneutrinos is in principle possible, especially since more channels would be kinematically allowed and the relic abundance could be obtained for moderate values of λ_N . Notice that, in order to do so, the mass of the neutralino (and that of the rest of the spectrum) also must be increased so that the right-handed sneutrino is the LSP. This can be done through an increase in the gaugino and scalar mass parameters as well as in the μ term. However, this entails a further reduction of the supersymmetric contribution to the muon anomalous magnetic moment, thereby increasing the tension with its experimental bound.

4 Direct detection

The direct detection of sneutrinos could take place through their elastic scattering with nuclei inside a dark matter detector. The interaction occurs in the non-relativistic regime (given that the velocity of sneutrinos in the dark matter halo is very small) and therefore one can easily find a description in terms of an effective Lagrangian. In our case, there is only one diagram contributing (at tree level) to this process, namely, the t -channel exchange of neutral Higgses shown in Fig. 14 (the exchange of a Z boson is largely suppressed by the neutrino Yukawa squared and therefore is

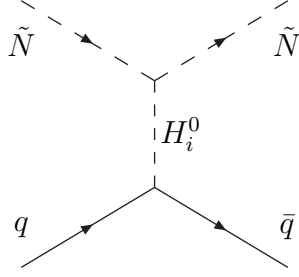


Figure 14: Diagram describing the elastic interaction of sneutrinos with quarks.

completely negligible). The effective Lagrangian describing the four-field interaction only contains a scalar coupling which reads

$$\mathcal{L}_{eff} \supset \alpha_{q_i} \tilde{N} \tilde{N} \bar{q}_i q_i \quad (4.25)$$

with

$$\alpha_{q_i} \equiv \sum_{j=1}^3 \frac{C_{H_i^0 \tilde{\nu} \tilde{\nu}} Y_{q_i}}{m_{H_i^0}^2} \quad (4.26)$$

where $C_{H_i^0 \tilde{\nu} \tilde{\nu}}$ is defined in Appendix A, Y_{q_i} is the corresponding quark Yukawa coupling and i labels up-type quarks ($i = 1$) and down-type quarks ($i = 2$). Notice that the effective Lagrangian contains no axial-vector coupling since the sneutrino is a scalar field, therefore implying a vanishing contribution to the spin-dependent cross section. The total spin-independent sneutrino-proton scattering cross section yields

$$\sigma_{\tilde{N}p}^{\text{SI}} = \frac{1}{\pi} \frac{m_p^2}{(m_p + m_{\tilde{N}_1})^2} f_p^2, \quad (4.27)$$

where m_p is the proton mass and

$$\frac{f_p}{m_p} = \sum_{q_i=u,d,s} f_{Tq_i}^p \frac{\alpha_{q_i}}{m_{q_i}} + \frac{2}{27} f_{TG}^p \sum_{q_i=c,b,t} \frac{\alpha_{q_i}}{m_{q_i}}. \quad (4.28)$$

The quantities $f_{Tq_i}^p$ and f_{TG}^p are the hadronic matrix elements which parametrize the quark content of the proton. They are subject to considerable uncertainties [66, 67, 68] which induce a significant correction to the theoretical predictions for $\sigma_{\tilde{N}p}^{\text{SI}}$. In our analysis we will consider the most recent values for these quantities, as explained in [69].

It is obvious from the previous formulae that the sneutrino detection cross section is extremely dependent on the features of the Higgs sector of the model. In particular, $\sigma_{\tilde{N}p}^{\text{SI}}$

becomes larger when the sneutrino-sneutrino-Higgs coupling increases (which according to its expression in Appendix A can be achieved by enhancing λ_N or with large values for $|A_{\lambda_N}|$). Moreover, from Eq. (4.26) we also see that larger values $\sigma_{\tilde{N}p}^{\text{SI}}$ can be obtained in those regions of the parameter space where the mass of the lightest Higgs becomes smaller.

We will now calculate the theoretical predictions for the sneutrino scattering cross section for the various cases studied in Section 3. Let us begin by addressing case A) in Table 1, for which we have seen in Section 3.1.1 that the $H_1^0 H_1^0$ channel is the dominant contribution to the annihilation cross section for moderate values of λ_N . Choosing $A_{\lambda_N} = -250$ GeV and performing the same scan in λ_N and $m_{\tilde{N}}$ as in Fig. 4 we have calculated the resulting sneutrino scattering cross section off quarks in those cases where the sneutrino abundance is consistent with the WMAP constraint or smaller (in which case the sneutrino could be a subdominant dark matter component).

If the sneutrino only contributes to a fraction of the total dark matter density, one should expect that it is present in the dark matter halo in the same proportion as in the Universe, contributing only to a fraction of the local dark matter density. This implies, of course, a reduction of the detection rate in direct detection experiments. In order to take this effect into account, it is customary to define the sneutrino fractional density $\xi = \min[1, \Omega_{\tilde{N}} h^2 / 0.1037]$ [50] and plot the modulated elastic scattering cross section, $\xi \sigma_{\tilde{N}p}^{\text{SI}}$.

We follow this approach and show on the left-hand side of Fig. 15 the theoretical predictions for the spin-independent contribution to $\xi \sigma_{\tilde{N}p}^{\text{SI}}$ as a function of the sneutrino mass for the example studied in Section 3.1.1. This is, case A) with $A_{\lambda_N} = -250$ GeV, $\lambda_N \in [0.05, 0.1]$ and $m_{\tilde{N}} \in [0, 250]$ GeV. Black dots correspond to points with a relic density consistent with the WMAP results, whereas grey dots stand for those with $\Omega_{\tilde{N}} h^2 \leq 0.1037$.

For light sneutrinos, for which annihilation into Higgses is not kinematically allowed, the value of λ_N in order to have the correct relic density is large (see Fig. 5). Consequently, the resulting scattering cross section turns out to be sizable and easily exceeds the sensitivities of present detectors. On the other hand, when annihilation into CP-even Higgses is possible, the necessary value of λ_N is smaller, of order 0.1, resulting in $\xi \sigma_{\tilde{N}p}^{\text{SI}} \lesssim 10^{-8}$ pb. These results are not yet excluded by present searches, but interestingly, could be within the reach of future experiments such as SuperCDMS. Notice also that along the Higgs resonances the sneutrino scattering cross section decreases considerably since the necessary value of the λ_N coupling to obtain the correct

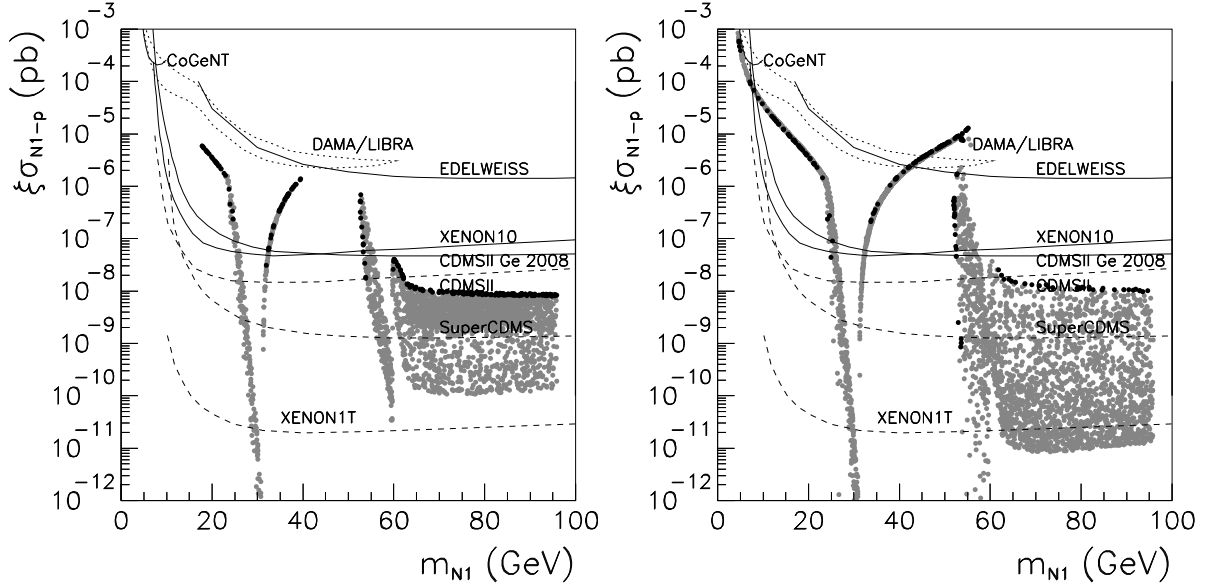


Figure 15: Theoretical predictions for $\xi\sigma_{Np}^{\text{SI}}$, as a function of the sneutrino mass for example A) of Table 1. All the points represented fulfil all the experimental constraints. Black dots correspond to those which reproduce the WMAP result for the dark matter relic density whereas grey ones represent those with $\Omega_{\tilde{N}} h^2 < 0.1037$. The sensitivities of present and projected experiments are represented by means of solid and dashed lines, respectively, in the case of an isothermal spherical halo. The large (small) area bounded by dotted lines is consistent with the interpretation of DAMA experiment in terms of a WIMP.

relic density becomes much smaller.

On the right-hand side of Fig. 15 we show the results for case A) but for $A_{\lambda_N} = -500$ GeV, which corresponds to the case analysed in Section 3.1.2. We remind the reader that in this example a larger λ_N was allowed and we perform a scan in $\lambda_N \in [0.05, 0.35]$ with $m_{\tilde{N}} \in [0, 250]$ GeV. This made it possible to obtain very light sneutrinos with the correct relic abundance. The large value of λ_N implies that the detection cross section for these light sneutrinos is also very large. This is clearly evidenced in the plot, where we find that sneutrinos lighter than 20 GeV have a cross section which can be as large as $\xi\sigma_{Np}^{\text{SI}} \sim 10^{-4}$ pb.

This situation is very similar to what happens with very light neutralinos in the MSSM. Very light neutralinos with masses $m_{\tilde{\chi}_1^0} \gtrsim 7$ GeV can be obtained [51, 52] if the GUT relation for gaugino masses is abandoned. Although it was argued that these neutralinos could account for the DAMA/LIBRA annual modulation signal without

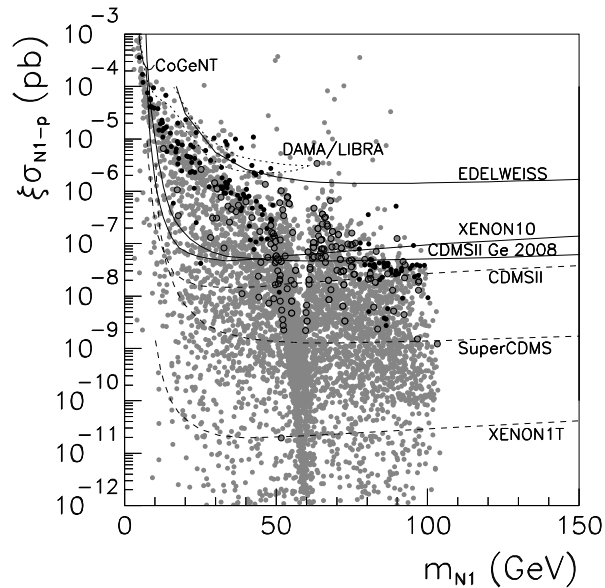


Figure 16: The same as in Fig.15 but for a scan in the (λ, κ) plane. Empty circles correspond to points with the correct relic abundance due to resonant annihilation effects.

contradicting the null results from CDMS and XENON10 [53], this interpretation is now more constrained by the recent results published by the MAJORANA collaboration using results from low-threshold experiments [54].

Finally, in order to explore more general variations in the NMSSM parameters, we have scanned in the allowed (λ, κ) plane, keeping $A_{\lambda_N} = -500$ GeV and the same scan in the λ_N and $m_{\tilde{N}}$ parameters as in the previous case. As we see from the resulting cross section, depicted in Fig. 16 where we see again that the cross section can be rather large (especially in those cases with light CP-even Higgs bosons). The region with very light sneutrinos, for with the predicted σ_{Np}^{SI} is sizable, could be within the reach of low-threshold experiments.

Next we address the examples B1) and B2) studied in Section 3.1.3, and for which annihilation into pseudoscalar Higgses was predominant. The results for the sneutrino scattering cross section are illustrated in Fig. 17.

We find a very different behaviour from the previous examples. First, since light sneutrinos are in this case obtained thanks to their annihilation into very light pseudoscalars, the value of λ_N at which the WMAP result is reproduced is considerably smaller. Second, the mass of the CP-even Higgs bosons is larger in this example than

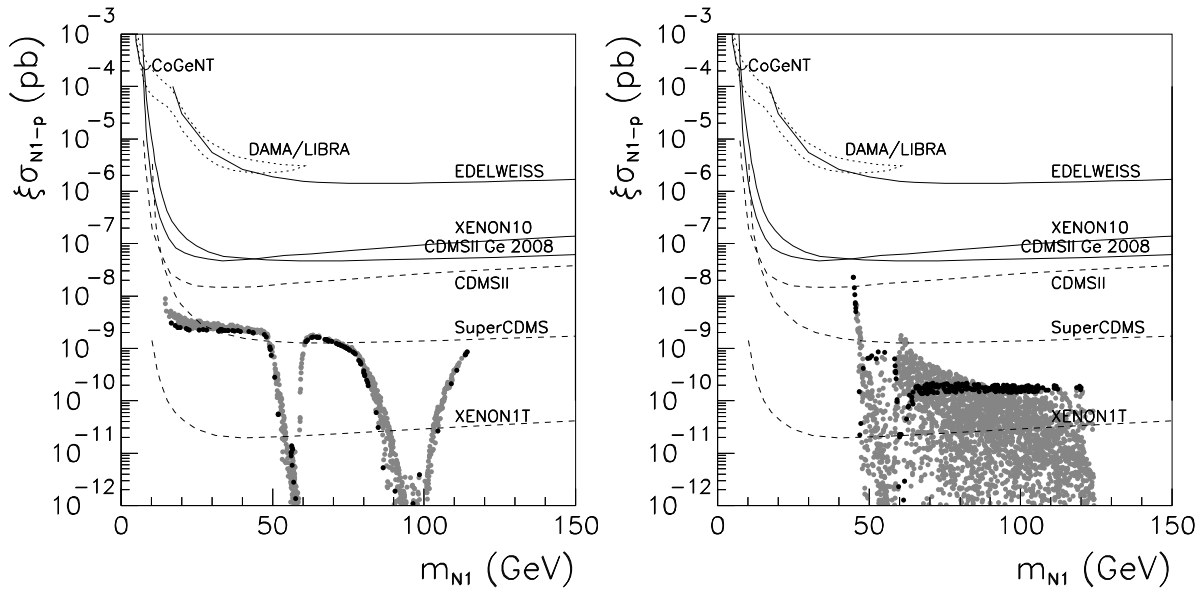


Figure 17: The same as in Fig. 15 but for examples B1) and B2) of Table 1.

in the previous one. As a consequence, these very light sneutrinos have a smaller scattering cross section and can evade the experimental constraints from XENON10 and CDMS.

For example, on the left-hand side of Fig. 17 (which corresponds to the case analysed in Fig. 7) sneutrinos as light as $m_{\tilde{N}_1} \sim 15$ GeV are obtained with the correct relic abundance and with a scattering cross section of order $\xi\sigma_{\tilde{N}p}^{\text{SI}} \approx 2 \times 10^{-9}$ pb. This is a very interesting situation, since as we will explain later in more detail, it is a completely different behaviour than the one observed for neutralinos in the MSSM.

On the right hand-side of Fig. 17 we show the results corresponding to the case analysed in Fig. 9). In this example the CP-even Higgs is heavier than in the previous examples and as a consequence we observe a decrease in the scattering cross section. In this case $\xi\sigma_{\tilde{N}p}^{\text{SI}} \lesssim 10^{-9}$ pb and Ton-scale detectors, such as the projected XENON1T would be necessary to explore them.

For completeness we have also performed a scan in the (λ, κ) plane, the results of which are shown on Fig. 18. Depending on the point of the (λ, κ) plane, the mass and coupling of the lightest pseudoscalar varies and the predictions for sneutrino dark matter are seriously affected. As a consequence, the predicted cross section for very light sneutrinos spans several orders of magnitude, ranging from 10^{-11} pb to 10^{-6} pb.

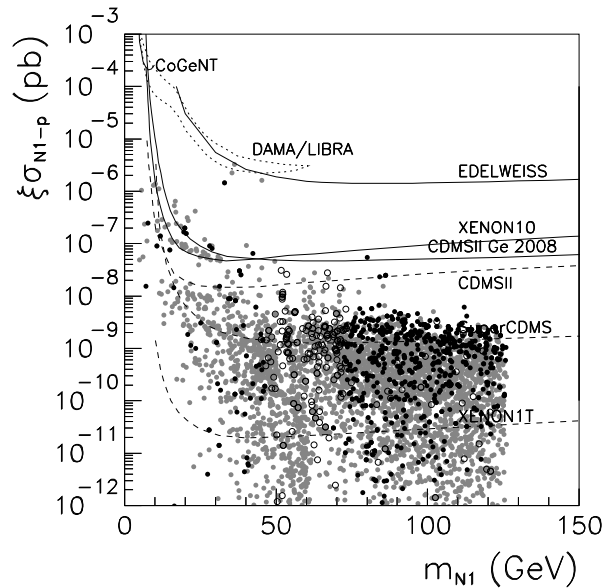


Figure 18: The same as in Fig. 17 but for a scan in the (λ, κ) plane.

Interestingly very light sneutrinos populate an area of the $\sigma_{Np}^{\text{SI}} - m_{\tilde{N}_1}$ plane which is forbidden to neutralinos in the MSSM. However, the predictions for very light neutralinos in the NMSSM are very similar to those obtained here for sneutrinos [54].

Finally let us address an example which we already studied in Section 3.1.4 and for which annihilation into a pair of right-handed neutrinos was the predominant sneutrino annihilation channel. In particular, we take the NMSSM parameters as in case C) of Table 1 with $A_{\lambda_N} = -250$ GeV. This correspond to the example studied in Figs. 12 and 13. In this example the mass of the scalar Higgses is rather large and therefore the resulting scattering cross section is reduced. The predictions are plotted in Fig. 19 as a function of the sneutrino mass and, as we can see, they are of order 2×10^{-9} pb. Once more, this result is not excluded by present dark matter searches and can be within the reach of some of the future experiments.

4.1 Overview and comparison with neutralino dark matter

We have so far shown that the right-handed sneutrino can be a viable WIMP in this construction. The examples throughout this Section illustrate how sneutrinos within a mass range of $m_{\tilde{N}_1} \approx 5 - 200$ GeV and satisfying the WMAP constraint can be

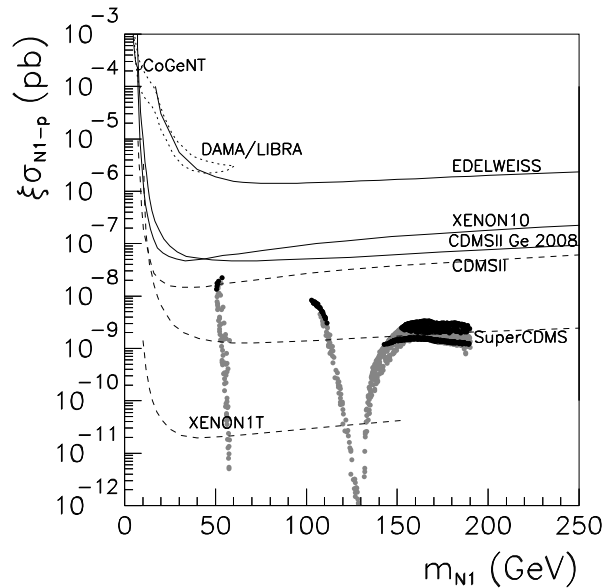


Figure 19: The same as in Fig. 15 but for example C) of Table 1.

obtained for which the predicted scattering cross section is not excluded by current experimental searches (unlike in the case of the left-handed sneutrino in the MSSM). Interestingly, the predicted σ_{Np}^{SI} is generally within the reach of future experiments, except along the Higgs resonances in which case the predicted scattering cross section can even be below the sensitivity of Ton-scale detectors.

We can combine the results of this Section in order to determine the region in the $(\sigma_{Np}^{\text{SI}}, m_{\tilde{N}_1})$ plane that the right-handed sneutrino can cover. This is helpful in order to understand in which regions could it account for a hypothetical WIMP detection in the future. We do this in Fig. 20, which is constructed gathering all the predictions from this Section, and which serves as a summary of our results.

This also allows us to compare with the predictions for other existing WIMPs. In particular, it should be pointed out that the area shown in Fig. 20 is within the area predicted for neutralinos in the NMSSM [30, 54] (as well as for neutralinos in the MSSM except for the region for very light WIMPs). One may therefore wonder whether these two candidates can be discriminated in the case of a hypothetical detection of dark matter. It should be pointed out in this respect that since the sneutrino has no spin-dependent couplings, the combination of data from two experiments whose targets are sensitive to spin-dependent and -independent couplings could be used to disentangle

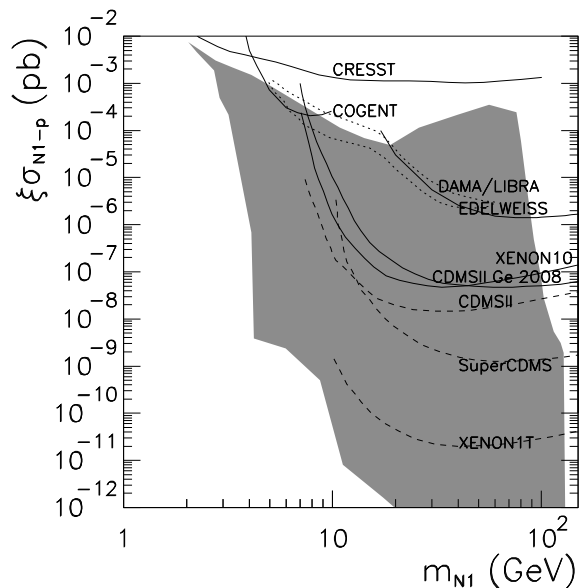


Figure 20: Combination of all the theoretical results for the sneutrino elastic scattering cross section as a function of the sneutrino mass.

between sneutrino and neutralino dark matter in the same way that it was shown for Kaluza-Klein dark matter and neutralinos in Ref. [55].

5 Implication for collider physics

Finally, we briefly comment on the characteristic signals that might be expected from this model at accelerator experiments.

As with other WIMP models, right-handed sneutrinos can be pair-produced in a collider and subsequently escape undetected. This would manifest as events with a deficit of transverse momentum. Notice that one expects the same kind of signals if the neutralino is the LSP and a dark matter candidate. Thus, the relevant question is whether or not the identity of the missing particle (sneutrino or neutralino) can be determined. An obvious difference between both particles is their spin. In this sense, the study of certain kinematic variables can give us some insight not only about the mass of the LSP [56], but even about its spin [57]. This would also be similar to the way the nature of the NLSP can be determined in scenarios of gravitino dark matter [58]. This, however might not be possible in the Large Hadron Collider and one would need

to wait for the International Linear Collider. Another crucial difference between the sneutrino and the neutralino is their lepton number. This was exploited in scenarios of sneutrino NLSP with gravitino LSP by studying the associated lepton production [70, 71]. However, this is not directly applicable to our case, since we are dealing with a pure right-handed sneutrino.

Nevertheless, there exists yet another attractive possibility, the production of right-handed neutrinos. These can be produced by the decay of either a Higgs boson or a neutralino (which can be the NLSP and decay into a sneutrino LSP and a right-handed neutrino). Once the right-handed neutrino is produced, it would be long-lived and decay, through the tiny mixing with the left-handed component, into a W boson and a charged lepton. This would give rise to a displaced vertex which could be observed.

As we have already stressed, sneutrino dark matter is very sensitive to the properties of the Higgs sector. When a Higgs boson with significant singlet component decays, depending on its mass, a pair of LSP right-handed sneutrinos and a pair of right-handed neutrinos, in other words the missing momentums and long-lived particles, are simultaneously produced. This is also a possible unique signal.

There is another interesting consequence, namely the invisible decay of the Higgs boson, since the right-handed sneutrino interacts with the CP-even Higgs through the coupling $C_{H_i^0 \tilde{\nu} \tilde{\nu}}$. This is a common feature of dark matter particles which predominantly annihilate through s -channel Higgs exchange and can be detected through t -channel Higgs exchange [72, 73].

In addition, through collider studies, it is possible to discriminate our model from other models with thermal right-handed sneutrino dark matter. In particular, there exists a family of models in which thermal right-handed neutralino dark matter is viable thanks to the inclusion of a new gauge interaction through a $U(1)'$ [19] or $U(1)_{B-L}$ [20]. These scenarios present a Z' gauge boson which is not present in our construction. The detection or not of this Z' would discriminate among these models. Also, another construction in which the Higgs sector is extended was presented in Ref. [23]. The essential difference with our scenario is that the singlet Higgs in that model [21, 23] is quite heavy and exchanging Higgs particles are $SU(2)$ doublet only. As a result, the correct relic abundance can only be realized with the help of the resonant annihilation. Hence, a strong correlation between the sneutrino mass and the Higgs mass is present. In addition, the right-handed neutrino production is only through the neutralino decay because of too heavy singlet Higgs. Thus, by examining the way of right-handed neutrino production, we may discriminate between these two models.

6 Conclusions

We have investigated the properties of the right-handed sneutrino and its viability as a WIMP dark matter candidate in an extended version of the NMSSM in which a right-handed neutrino superfield is included with a coupling to the scalar Higgs in order to provide a Majorana right-handed neutrino mass. Both the μ parameter and the neutrino Majorana mass are generated by the vacuum expectation value of the singlet field after radiative electroweak symmetry breaking and are therefore naturally of order of the electroweak scale. This implies small values for the neutrino Yukawas, of order of the electron Yukawa coupling and therefore leads to negligible mixing terms in the sneutrino mass matrix and to pure left- and right-handed mass eigenstates. The sneutrino spectrum is then analysed in terms of the three new parameters, the sneutrino-Higgs coupling λ_N , the sneutrino soft mass $m_{\tilde{N}}$ and the new trilinear term A_{λ_N} .

We compute the thermal relic abundance for the right-handed sneutrino, including all possible annihilation channels. The annihilation cross section is extremely dependent on the Higgs sector of the NMSSM. Interestingly, light CP-even and light CP-odd Higgses are viable in this model as in the NMSSM (if they have a large singlet component) and this provides interesting properties for the sneutrino. In particular, annihilation into light Higgses (scalar or pseudoscalar) makes it possible to reproduce the WMAP result for the relic abundance for low values of the sneutrino mass. We study the relevance of each individual annihilation channel and show how sneutrinos in the mass range 5-200 GeV can reproduce the correct value for the relic abundance for natural values of the three new parameters, $\lambda_N = \mathcal{O}(0.1)$, $m_{\tilde{N}} = \mathcal{O}(100)$ GeV and $|A_{\lambda_N}| = \mathcal{O}(250 - 500)$ GeV.

Next, the sneutrino-proton elastic scattering cross section is computed and compared with present experimental sensitivities. We find that the sneutrino is not ruled out by current searches for dark matter. Interestingly, many regions of the parameter space could be within the reach of some of the future dark matter experiments.

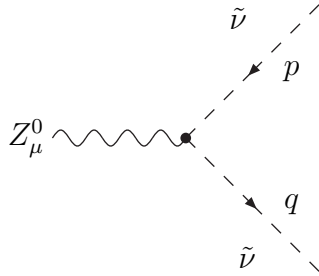
Finally, we commented on the possible implications for collider physics, identifying some potentially interesting signals. We discuss how, in some cases, our construction can be distinguished experimentally from other models for sneutrino dark matter as well as from other dark matter candidates such as the neutralino.

Acknowledgments

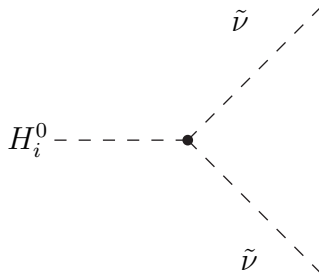
We have greatly benefited from discussions with T. Asaka, A. Ibarra and C. Muñoz. D.G.C. was supported by the program “Juan de la Cierva” of the Spanish MEC. and also in part by the Spanish DGI of the MEC under Proyecto Nacional FPA2006-01105, and by the EU network MRTN-CT-2006-035863. O.S. was partly supported by the MEC project FPA 2004-02015 and DOE grant DE-FG02-94ER-40823. We thank the ENTApP Network of the ILIAS project RII3-CT-2004-506222 and the project HEPHACOS P-ESP-00346 of the Comunidad de Madrid.

A Feynman rules

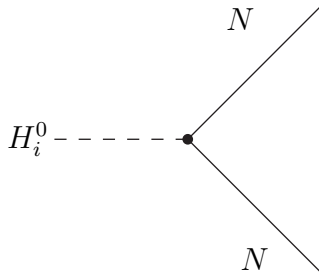
In this appendix we indicate the relevant vertices for the calculation of the sneutrino annihilation cross section. The couplings relevant to our computation and which receive contributions from the right-handed sneutrino sector we have introduced read



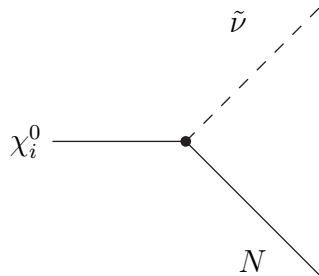
$$-\frac{ig}{\cos\theta_W} (p+q)^\mu (N_{i\tilde{\nu}_L}^\nu)^2$$



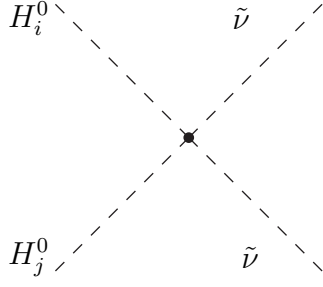
$$\begin{aligned} &-\frac{igM_Z}{2\cos\theta_W} (\cos\beta S_{H_i^0}^1 - \sin\beta S_{H_i^0}^2) (N_{i\tilde{\nu}_L}^\nu)^2 + \\ &i \left[\frac{2\lambda\lambda_N M_W}{\sqrt{2}g} (\sin\beta S_{H_i^0}^1 + \cos\beta S_{H_i^0}^2) + \right. \\ &\left. \left[(4\lambda_N^2 + 2\kappa\lambda_N) v_s + \lambda_N \frac{A_{\lambda_N}}{\sqrt{2}} \right] (S_{H_i^0}^3)^2 \right] (N_{i\tilde{\nu}_R}^\nu)^2 \\ &\equiv iC_{H_i^0\tilde{\nu}\tilde{\nu}} \end{aligned}$$



$$-\frac{i\lambda_N}{\sqrt{2}} (S_{H_i^0}^3) \equiv C_{NNH_i^0}$$

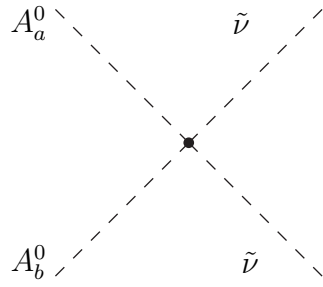


$$-i\sqrt{2}\lambda_N (N_{\tilde{\chi}_i^0}^\nu) (N_{i\tilde{\nu}}^\nu) \equiv C_{\tilde{\nu}N\tilde{\chi}_i^0}$$



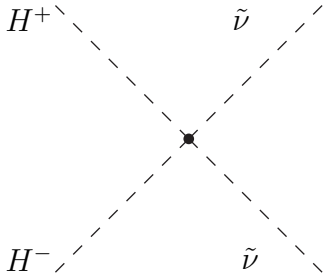
$$i \left(\frac{\lambda \lambda_N}{2} (S_{H_i^0}^1 S_{H_j^0}^2 + S_{H_i^0}^2 S_{H_j^0}^1) - \lambda_N (\kappa + 2\lambda_N) S_{H_i^0}^3 S_{H_j^0}^3 \right) (N_{i\tilde{N}}^{\tilde{\nu}})^2$$

$$\equiv i C_{H_i^0 H_j^0 \tilde{\nu} \tilde{\nu}}$$



$$-i \left(\frac{\lambda \lambda_N}{2} (P_{A_a^0}^1 P_{A_b^0}^2 + P_{A_a^0}^2 P_{A_b^0}^1) + \lambda_N (2\lambda_N - \kappa) P_{A_a^0}^3 P_{A_b^0}^3 \right) (N_{i\tilde{N}}^{\tilde{\nu}})^2$$

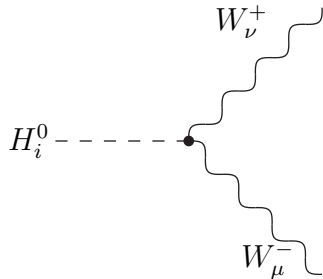
$$\equiv i C_{A_a^0 A_b^0 \tilde{\nu} \tilde{\nu}}$$



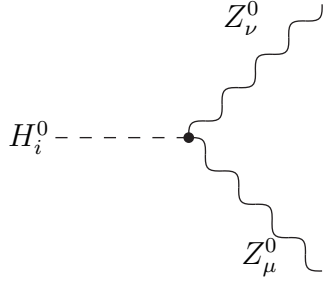
$$-i 2\lambda \lambda_N (N_{i\tilde{N}}^{\tilde{\nu}})^2$$

$$\equiv i C_{H^+ H^- \tilde{\nu} \tilde{\nu}}$$

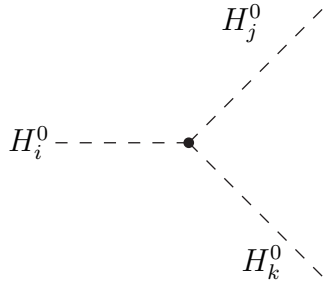
We will be also using the following usual NMSSM Feynman diagrams.



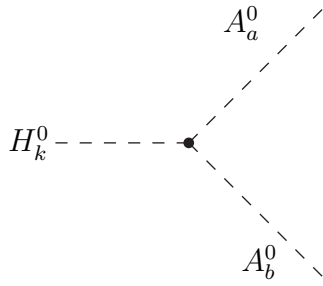
$$ig M_W (\cos \beta S_{H_i^0}^1 + \sin \beta S_{H_i^0}^2) g^{\mu\nu} \equiv ig M_W C_{H_i} g^{\mu\nu}$$



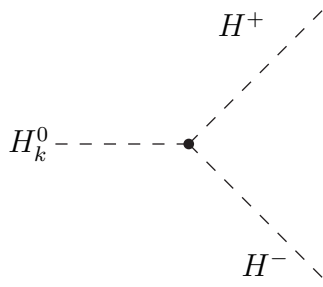
$$\frac{igM_Z}{\cos\theta_W} \left(\cos\beta S_{H_i^0}^1 + \sin\beta S_{H_i^0}^2 \right) g^{\mu\nu} \equiv \frac{igM_Z}{\cos\theta_W} C_{H_i} g^{\mu\nu}$$



$$\equiv iC_{H_i^0 H_j^0 H_k^0}$$



$$\equiv iC_{A_a^0 A_b^0 H_k^0}$$



$$\equiv iC_{H^+ H^- H_k^0}$$

$$\equiv iC_{H_k^0 A_a^0 Z}$$

$$\equiv iC_{H_k^0 H^+ W^-}$$

The explicit expressions for the couplings $C_{H_i^0 H_j^0 H_k^0}$, $C_{A_a^0 A_b^0 H_k^0}$, $C_{H^+ H^- H_k^0}$, $C_{H_k^0 A_a^0 Z}$, and $C_{H_k^0 H^+ W^-}$ can be found in [59], and translated into our formalism by doing the transformations $v_{1,2} \rightarrow \frac{v_{1,2}}{\sqrt{2}}$ and $v_s \rightarrow \frac{v_s}{\sqrt{2}}$.

B Annihilation channels

In order to determine the total annihilation cross section we follow the procedure of [38] and start by introducing a Lorentz-invariant function $w(s)$ [60]

$$w(s) = \frac{1}{4} \int d\text{LIPS} |\mathcal{A}(\tilde{N}\tilde{N} \rightarrow \text{all})|^2 \quad (\text{B.29})$$

where $|\mathcal{A}(\tilde{N}\tilde{N} \rightarrow \text{all})|^2$ denotes the absolute square of the reduced matrix element for the annihilation of two sneutrinos, averaged over initial spins and summed over final spins. The function $w(s)$ is related to the annihilation cross section $\sigma(s)$ via [61]

$$w(s) = \frac{1}{2} \sqrt{s(s - 4m_{\tilde{N}_1}^2)} \sigma(s). \quad (\text{B.30})$$

Since $w(s)$ receives contributions from all the kinematically allowed annihilation process $\tilde{N}\tilde{N} \rightarrow X_1X_2$, it can be written as

$$w(s) = \frac{1}{32\pi} \sum_{X_1X_2} \left[c \theta(s - (m_{X_1} + m_{X_2})^2) \beta_X(s, m_{X_1}, m_{X_2}) \tilde{w}_{X_1X_2}(s) \right], \quad (\text{B.31})$$

where the summation extends over all possible two-body final states X_1X_2 , m_{X_1} and m_{X_2} denote their respective masses, and

$$c = \begin{cases} c_f & \text{if } X_{1(2)} = f(\bar{f}) \\ 1 & \text{otherwise,} \end{cases} \quad (\text{B.32})$$

where c_f is the color factor of SM fermions ($c_f = 3$ for quarks and $c_f = 1$ for leptons). The kinematic factor β_X is defined as

$$\beta_X(s, m_{X_1}, m_{X_2}) \equiv \left[1 - \frac{(m_{X_1} + m_{X_2})^2}{s} \right]^{1/2} \left[1 - \frac{(m_{X_1} - m_{X_2})^2}{s} \right]^{1/2}. \quad (\text{B.33})$$

In the CM frame, which we choose for convenience, the function $\tilde{w}_{X_1X_2}(s)$ can be expressed as

$$\tilde{w}_{X_1X_2}(s) \equiv \frac{1}{2} \int_{-1}^{+1} d\cos\theta_{CM} |\mathcal{A}(\tilde{N}\tilde{N} \rightarrow X_1X_2)|^2, \quad (\text{B.34})$$

where θ_{CM} denotes the scattering angle in the CM frame. In other words, we write $|\mathcal{A}(\tilde{N}\tilde{N} \rightarrow X_1X_2)|^2$ as a function of s and $\cos\theta_{CM}$, which greatly simplifies the computation.

We present here the analytic expressions for the \tilde{w} functions for the various annihilation channels. In doing so, we have assumed the lightest sneutrino to be a pure right-handed sneutrino, hence $N_{\tilde{\nu}_L}^{\tilde{\nu}} = 0$ and $N_{i\tilde{N}}^{\tilde{\nu}} = 1$ with $i = 1$.

In the following expressions we define

$$\Delta_i \equiv (s - m_{H_i^0}^2) + \frac{(m_{H_i^0} \Gamma_i)^2}{s - m_{H_i^0}^2}, \quad (\text{B.35})$$

$$\begin{aligned} \Delta_{ij} \equiv & (s - m_{H_i^0}^2)(s - m_{H_j^0}^2) + m_{H_i^0} m_{H_j^0} \Gamma_i \Gamma_j \\ & + \frac{(m_{H_i^0} \Gamma_i (s - m_{H_j^0}^2) - m_{H_j^0} \Gamma_j (s - m_{H_i^0}^2))^2}{(s - m_{H_i^0}^2)(s - m_{H_j^0}^2) + m_{H_i^0} m_{H_j^0} \Gamma_i \Gamma_j}, \end{aligned} \quad (\text{B.36})$$

for $i, j = 1, 2, 3$, where Γ_i is the decay width of the Higgs H_i^0 .

- $\rightarrow W^+W^-$

The annihilation proceeds through an s -channel mediated by a scalar Higgs, H_i^0 .

$$\tilde{w}_{W^+W^-} = 6g^2 M_W^2 \sum_{i,j=1}^3 \frac{C_{H_i^0 \tilde{\nu}\tilde{\nu}} C_{H_j^0 \tilde{\nu}\tilde{\nu}} C_{H_i} C_{H_j}}{\Delta_{ij}} \quad (\text{B.37})$$

- $\rightarrow ZZ$

The annihilation proceeds through an s -channel mediated by a scalar Higgs, H_i^0 . The t -channels where a sneutrino is exchanged do not contribute since the $Z - \tilde{\nu} - \tilde{\nu}$ coupling vanishes for pure right-handed sneutrinos.

$$\tilde{w}_{ZZ} = \frac{3g^2 M_Z^2}{\cos \theta_W} \sum_{i,j=1}^3 \frac{C_{H_i^0 \tilde{\nu}\tilde{\nu}} C_{H_j^0 \tilde{\nu}\tilde{\nu}} C_{H_i} C_{H_j}}{\Delta_{ij}} \quad (\text{B.38})$$

- $\rightarrow H_i^0 H_j^0$

There are four contributions to this annihilation channel. One comes from an s -channel mediated by a scalar Higgs, H_k^0 , the t, u -channels where a sneutrino is exchanged, and the point interaction.

$$\begin{aligned}
\tilde{w}_{H_i H_j} = & 2(C_{H_i^0 H_j^0 \tilde{\nu}\tilde{\nu}})^2 - 4 \sum_{k=1}^3 \frac{C_{H_k^0 \tilde{\nu}\tilde{\nu}} C_{H_i^0 H_j^0 H_k^0}}{\Delta_k} + 2 \sum_{k,l=1}^3 \frac{C_{H_k^0 \tilde{\nu}\tilde{\nu}} C_{H_l^0 \tilde{\nu}\tilde{\nu}} C_{H_i^0 H_j^0 H_k^0} C_{H_i^0 H_j^0 H_l^0}}{\Delta_{kl}} + \\
& \frac{2(C_{H_i^0 \tilde{\nu}\tilde{\nu}} C_{H_j^0 \tilde{\nu}\tilde{\nu}})^2 (A_{H_i^0}^t + A_{H_i^0}^u)^2}{A_{H_i^0}^t{}^2 A_{H_i^0}^u{}^2 E_{H_i^0}{}^2 s} \left[\frac{B_{H_i^0}^t B_{H_i^0}^u}{(B_{H_i^0}^t + B_{H_i^0}^u)^3} + \right. \\
& \left. \frac{(B_{H_i^0}^t{}^2 + B_{H_i^0}^u{}^2) - (B_{H_i^0}^t B_{H_i^0}^u)^2}{(1 - B_{H_i^0}^t{}^2)(1 - B_{H_i^0}^u{}^2)(B_{H_i^0}^t + B_{H_i^0}^u)^2} \right] + \\
& 2 \sum_{k=1}^3 \frac{C_{H_i^0 H_j^0 H_k^0} C_{H_i^0 \tilde{\nu}\tilde{\nu}} C_{H_j^0 \tilde{\nu}\tilde{\nu}} C_{H_k^0 \tilde{\nu}\tilde{\nu}} (A_{H_i^0}^t + A_{H_i^0}^u)}{A_{H_i^0}^t A_{H_i^0}^u E_{H_i^0} \sqrt{s} \Delta_k} \left[\frac{\mathcal{F}_1(B_{H_i^0}^t) + \mathcal{F}_1(B_{H_i^0}^u)}{B_{H_i^0}^t + B_{H_i^0}^u} \right] - \\
& 2 \frac{C_{H_i^0 \tilde{\nu}\tilde{\nu}} C_{H_j^0 \tilde{\nu}\tilde{\nu}} C_{H_i^0 H_j^0 \tilde{\nu}\tilde{\nu}} (A_{H_i^0}^t + A_{H_i^0}^u)}{A_{H_i^0}^t A_{H_i^0}^u E_{H_i^0} \sqrt{s}} \left[\frac{\mathcal{F}_1(B_{H_i^0}^t) + \mathcal{F}_1(B_{H_i^0}^u)}{B_{H_i^0}^t + B_{H_i^0}^u} \right] \quad (\text{B.39})
\end{aligned}$$

which should be multiplied by a factor 1/2 in the case of identical particles in the final state.

We have defined

$$\mathcal{F}_1(x) \equiv \log \left(\frac{1+x}{1-x} \right) \quad (\text{B.40})$$

$$A_{H_i^0}^t \equiv \frac{m_{H_i^0}^2}{\sqrt{s} E_{H_i^0}} - 1 \quad (\text{B.41})$$

$$A_{H_i^0}^u \equiv \frac{m_{H_j^0}^2 - s}{\sqrt{s} E_{H_i^0}} + 1 \quad (\text{B.42})$$

and

$$B_{H_i^0}^t \equiv \frac{\sqrt{\frac{s}{4} - m_{\tilde{N}_1}^2} \sqrt{E_{H_i^0}^2 - m_{H_i^0}^2}}{m_{H_i^0}^2 - \sqrt{s} E_{H_i^0}} \quad (\text{B.43})$$

$$B_{H_i^0}^u \equiv \frac{\sqrt{\frac{s}{4} - m_{\tilde{N}_1}^2} \sqrt{E_{H_i^0}^2 - m_{H_i^0}^2}}{m_{H_j^0}^2 - s + \sqrt{s} E_{H_i^0}} \quad (\text{B.44})$$

where

$$E_{H_i^0} = \frac{s - (m_{H_j^0}^2 - m_{H_i^0}^2)}{2\sqrt{s}} \quad (\text{B.45})$$

$$E_{H_j^0} = \frac{s + (m_{H_j^0}^2 - m_{H_i^0}^2)}{2\sqrt{s}} \quad (\text{B.46})$$

• $\rightarrow A_a^0 A_b^0$

The annihilation proceeds through an s -channel mediated by a scalar Higgs, H_k^0 and a point interaction.

$$\begin{aligned} \tilde{w}_{A_a^0 A_b^0} &= 2(C_{A_a^0 A_b^0 \bar{\nu} \nu})^2 - 4 \sum_{k=1}^3 \frac{C_{A_a^0 A_b^0 \bar{\nu} \nu} C_{H_k^0 \bar{\nu} \nu} C_{A_a^0 A_b^0 H_k^0}}{\Delta_k} + \\ &2 \sum_{k,l=1}^3 \frac{C_{H_k^0 \bar{\nu} \nu} C_{H_l^0 \bar{\nu} \nu} C_{A_a^0 A_b^0 H_k^0} C_{A_a^0 A_b^0 H_l^0}}{\Delta_{kl}} \end{aligned} \quad (\text{B.47})$$

which is multiplied by a factor 1/2 in the case of identical particles in the final state.

• $\rightarrow f \bar{f}$

We only include here the s -channel mediated by a scalar Higgs, H_k^0 . Once more, the s -channel annihilation mediated by the Z boson vanishes for a pure right-handed sneutrino. For annihilation into $l \bar{l}$ ($\nu \bar{\nu}$) one should, in principle, also consider the t -channel mediated by charginos (neutralinos). However, those diagrams are suppressed by the very small Yukawa coupling, Y_N , and will be here neglected.

$$\tilde{w}_{f \bar{f}} = 2 \sum_{i,j=1}^3 \frac{C_{H_i^0 \bar{\nu} \nu} C_{H_j^0 \bar{\nu} \nu} C_{f H_i^0} C_{f H_j^0}}{\Delta_{ij}} (2s - 8m_f^2) \quad (\text{B.48})$$

• $\rightarrow NN$

There are three contributions to this channel, namely the s -channel, mediated by a scalar Higgs, H_k^0 , together with the t - and u - channels where (the five) neutralinos are exchanged.

First, we address the case where the lightest sneutrino is the real part of right-handed sneutrino.

$$\tilde{w}_{NN} = w_{NN}^s + w_{NN}^{st,su} + w_{NN}^{t,u}, \quad (\text{B.49})$$

with

$$\tilde{w}_{NN}^s = \sum_{k,l=1}^3 \frac{C_{H_k^0 \tilde{\nu} \tilde{\nu}} C_{H_1^0 \tilde{\nu} \tilde{\nu}} C_{NNH_k^0} C_{NNH_1^0}}{\Delta_{kl}} (s - 4M_N^2) \quad (\text{B.50})$$

$$\tilde{w}_{NN}^{st,su} = \sum_{k=1}^3 \sum_{i=1}^5 \frac{8C_{H_k^0 \tilde{\nu} \tilde{\nu}} C_{NNH_k^0} (C_{\tilde{\nu} N \tilde{\chi}_i})^2}{\Delta_k} \left[-M_N + \frac{\mathcal{D}(m_{\tilde{\chi}_i})}{2A} \log \left(\frac{A_i + A}{A_i - A} \right) \right] \quad (\text{B.51})$$

$$\begin{aligned} \tilde{w}_{NN}^{t,u} = & \sum_{i=1}^5 \frac{32C_{\tilde{\nu} N \tilde{\chi}_i}^4}{s^2} \left[-\frac{s^2}{8} + \frac{\mathcal{A}(m_{\tilde{\chi}_i})}{(A_i^2 - A^2)} - \frac{\mathcal{B}(m_{\tilde{\chi}_i})}{2A_i A} \log \left(\frac{A_i - A}{A_i + A} \right) \right] + \\ & \sum_{i \neq j=1}^5 \frac{32C_{\tilde{\nu} N \tilde{\chi}_i}^2 C_{\tilde{\nu} N \tilde{\chi}_j}^2}{s^2} \left[-\frac{s^2}{8} - \frac{\mathcal{C}(m_{\tilde{\chi}_i}, m_{\tilde{\chi}_j})}{A(A_i^2 - A_j^2)} \log \left(\frac{A_i + A}{A_i - A} \right) + \right. \\ & \left. \frac{\mathcal{C}(m_{\tilde{\chi}_j}, m_{\tilde{\chi}_i})}{A(A_i^2 - A_j^2)} \log \left(\frac{A_j + A}{A_j - A} \right) \right] \end{aligned} \quad (\text{B.52})$$

The following auxiliary functions have been used

$$\begin{aligned} \mathcal{A}(m_{\tilde{\chi}_i}) \equiv & \left(\frac{s}{4} - m_N^2 \right) (m_N + m_{\tilde{\chi}_i})^2 + \frac{s}{4} \left(\frac{s}{4} - m_{\tilde{N}_1}^2 + 2m_N^2 A_i + 2m_N m_{\tilde{\chi}_i} A_i \right) - \\ & \frac{s^2}{16} A_i^2, \end{aligned} \quad (\text{B.53})$$

$$\begin{aligned} \mathcal{B}(m_{\tilde{\chi}_i}) \equiv & \left(\frac{s}{4} - m_N^2 \right) (m_N + m_{\tilde{\chi}_i})^2 - \frac{s}{4} \left(\frac{s}{4} - m_{\tilde{N}_1}^2 + 2m_N^2 A_i + 2m_N m_{\tilde{\chi}_i} A_i \right) + \\ & 3 \frac{s^2}{16} A_i^2, \end{aligned} \quad (\text{B.54})$$

$$\begin{aligned} \mathcal{C}(m_{\tilde{\chi}_i}, m_{\tilde{\chi}_j}) \equiv & \left(\frac{s}{4} - m_N^2 \right) (m_N + m_{\tilde{\chi}_i}) (m_N + m_{\tilde{\chi}_j}) A_j + \\ & \frac{s}{4} \left(\frac{s}{4} - m_{\tilde{N}_1}^2 + m_N^2 (A_i + A_j) + m_N (m_{\tilde{\chi}_i} A_i + m_{\tilde{\chi}_j} A_j) \right) A_i - \\ & \frac{s^2}{16} A_i^3 \end{aligned} \quad (\text{B.55})$$

$$\mathcal{D}(m_{\tilde{\chi}_i}) \equiv \left(1 - \frac{4M_N^2}{s} \right) (M_N + m_{\tilde{\chi}_i}) + M_N A_i \quad (\text{B.56})$$

We have also defined

$$A \equiv \frac{1}{s} \sqrt{s - 4m_{\tilde{N}_1}^2} \sqrt{s - 4m_N^2}, \quad (\text{B.57})$$

$$A_i \equiv 2 \frac{m_{\tilde{N}_1}^2 + m_N^2 - m_{\tilde{\chi}_i}^2}{s} - 1 \quad (\text{B.58})$$

In the case that the lightest sneutrino is the imaginary part of right-handed sneutrino, one can obtain the relevant \tilde{w}_{NN} by replacing

$$w_{NN}^{st,su} \rightarrow -w_{NN}^{st,su}, \quad (\text{B.59})$$

and

$$m_N \rightarrow -m_N \quad (\text{B.60})$$

in $w_{NN}^{t,u}$.

• $\rightarrow H^+H^-$

As in the case of annihilation into pseudoscalar Higgses, the annihilation receives contributions from an s -channel mediated by a scalar Higgs, H_k^0 and a point interaction.

$$\begin{aligned} \tilde{w}_{H^+H^-} = & 2(C_{H^+H^- \tilde{\nu}\tilde{\nu}})^2 - 4 \sum_{k=1}^3 \frac{C_{H^+H^- \tilde{\nu}\tilde{\nu}} C_{H_k^0 \tilde{\nu}\tilde{\nu}} C_{H^+H^- H_k^0}}{\Delta_k} + \\ & 2 \sum_{k,l=1}^3 \frac{C_{H_k^0 \tilde{\nu}\tilde{\nu}} C_{H_l^0 \tilde{\nu}\tilde{\nu}} C_{H^+H^- H_k^0}^2}{\Delta_{kl}} \end{aligned} \quad (\text{B.61})$$

• $\rightarrow ZA_a^0$

This channel receives contribution from s -channel scalar Higgs exchange. Notice that although there would also be an s -channel with Z boson mediation, the smallness of the Yukawa Y_N renders that contribution negligible.

$$\begin{aligned} \tilde{w}_{ZA_a^0} = & \sum_{k,l=1}^3 \frac{C_{H_k^0 \tilde{\nu}\tilde{\nu}} C_{H_l^0 \tilde{\nu}\tilde{\nu}} C_{H_k^0 A_a^0 Z} C_{H_l^0 A_a^0 Z}}{\Delta_{kl}} \\ & \left(-2s + M_Z^2 + 2m_{A_a^0}^2 + \frac{s^2 + m_{A_a^0}^4 - 2m_{A_a^0}^2 s}{M_Z^2} \right). \end{aligned} \quad (\text{B.62})$$

• $\rightarrow W^- H^+$

As in the case above, this channel receives contribution from s -channel scalar Higgs exchange.

$$\tilde{w}_{W^- H^+} = \sum_{k,l=1}^3 \frac{C_{H_k^0 \bar{\nu} \nu} C_{H_l^0 \bar{\nu} \nu} C_{H_k^0 H^+ W^-} C_{H_l^0 H^+ W^-}}{\Delta_{kl}} \left(-2s + M_W^2 + 2m_{H^+}^2 + \frac{s^2 + m_{H^+}^4 - 2m_{H^+}^2 s}{M_W^2} \right). \quad (\text{B.63})$$

References

- [1] G. Bertone, D. Hooper and J. Silk, Phys. Rept. **405** (2005) 279 [arXiv:hep-ph/0404175].
- [2] H. Goldberg, Phys. Rev. Lett. **50** (1983) 1419;
J. R. Ellis, J. S. Hagelin, D. V. Nanopoulos and M. Srednicki, Phys. Lett. B **127** (1983) 233;
J. R. Ellis, J. S. Hagelin, D. V. Nanopoulos, K. A. Olive and M. Srednicki, Nucl. Phys. B **238** (1984) 453.
- [3] G. Jungman, M. Kamionkowski and K. Griest, Phys. Rept. **267** (1996) 195 [arXiv:hep-ph/9506380].
- [4] L.E. Ibáñez, Phys. Lett. B **137** 160 (1984);
J.S. Hagelin, G.L. Kane and S. Raby, Nucl. Phys. B **241** 638 (1994).
- [5] For a recent review, see: C. Muñoz, Int. J. Mod. Phys. A**19** 3093 (2004).
- [6] T. Falk, K. A. Olive and M. Srednicki, Phys. Lett. B **339** (1994) 248 [arXiv:hep-ph/9409270].
- [7] L. J. Hall, T. Moroi and H. Murayama, Phys. Lett. B **424** (1998) 305 [arXiv:hep-ph/9712515].
- [8] C. Arina and N. Fornengo, JHEP **0711** (2007) 029 [arXiv:0709.4477 [hep-ph]].
- [9] For recent reviews, see e.g., R. N. Mohapatra *et al.*, Rept. Prog. Phys. **70**, 1757 (2007) [arXiv:hep-ph/0510213];
A. Strumia and F. Vissani, arXiv:hep-ph/0606054.
- [10] P. Minkowski, Phys. Lett. B **67** 421 (1977);
T. Yanagida, in *Proceedings of Workshop on the Unified Theory and the Baryon Number in the Universe*, Tsukuba, Japan, edited by A. Sawada and A. Sugamoto (KEK, Tsukuba, 1979), p 95;
M. Gell-Mann, P. Ramond, and R. Slansky, in *Supergravity*, Proceedings of Workshop, Stony Brook, New York, 1979, edited by P. Van Nieuwenhuizen and D. Z. Freedman (North-Holland, Amsterdam, 1979), p 315;
R. N. Mohapatra and G. Senjanovic, Phys. Rev. Lett. **44**, 912 (1980).

- [11] N. Arkani-Hamed, L. J. Hall, H. Murayama, D. R. Smith and N. Weiner, Phys. Rev. D **64** (2001) 115011 [arXiv:hep-ph/0006312].
- [12] D. Hooper, J. March-Russell and S. M. West, Phys. Lett. B **605** (2005) 228 [arXiv:hep-ph/0410114].
- [13] F. Borzumati and Y. Nomura, Phys. Rev. D **64** (2001) 053005 [arXiv:hep-ph/0007018].
- [14] C. Arina, F. Bazzocchi, N. Fornengo, J. C. Romao and J. W. F. Valle, arXiv:0806.3225.
- [15] T. Asaka, K. Ishiwata and T. Moroi, Phys. Rev. D **73** (2006) 051301 [arXiv:hep-ph/0512118], and Phys. Rev. D **75** (2007) 065001 [arXiv:hep-ph/0612211].
- [16] S. Gopalakrishna, A. de Gouvea and W. Porod, JCAP **0605** (2006) 005 [arXiv:hep-ph/0602027].
- [17] J. McDonald, JCAP **0701** (2007) 001 [arXiv:hep-ph/0609126].
- [18] V. Page, JHEP **0704** (2007) 021 [arXiv:hep-ph/0701266].
- [19] H. S. Lee, K. T. Matchev and S. Nasri, Phys. Rev. D **76** (2007) 041302 [arXiv:hep-ph/0702223].
- [20] R. Allahverdi, B. Dutta and A. Mazumdar, Phys. Rev. Lett. **99**, 261301 (2007) [arXiv:0708.3983 [hep-ph]].
- [21] B. Garbrecht, C. Pallis and A. Pilaftsis, JHEP **0612**, 038 (2006);
- [22] D. G. Cerdeño, C. Muñoz and O. Seto, Phys. Rev. D **79**, 023510 (2009) [arXiv:0807.3029 [hep-ph]].
- [23] F. Deppisch and A. Pilaftsis, arXiv:0808.0490 [hep-ph].
- [24] D. E. Kaplan, M. A. Luty and K. M. Zurek, arXiv:0901.4117 [hep-ph].
- [25] J. E. Kim and H. P. Nilles, Phys. Lett. B **138** (1984) 150.
- [26] L. E. Ibáñez and G. G. Ross, Phys. Lett. B **110** (1982) 215;
L. Alvarez-Gaume, M. Claudson and M. B. Wise, Nucl. Phys. B **207** (1982) 96;
K. Inoue, A. Kakuto, H. Komatsu and S. Takeshita, Prog. Theor. Phys. **67** (1982) 1889 and Prog. Theor. Phys. **68** (1982) 927 [Erratum-ibid. **70** (1983) 330].

- [27] H. P. Nilles, M. Srednicki and D. Wyler, Phys. Lett. B **120** (1983) 346;
 J. R. Ellis, J. F. Gunion, H. E. Haber, L. Roszkowski and F. Zwirner, Phys. Rev. D **39** (1989) 844;
 M. Drees, Int. J. Mod. Phys. A **4** (1989) 3635.
- [28] M. Bastero-Gil, C. Hugonie, S. F. King, D. P. Roy and S. Vempati, Phys. Lett. B **489** (2000) 359 [arXiv:hep-ph/0006198].
- [29] See, e.g., A. Djouadi *et al.*, JHEP **0807** (2008) 002 [arXiv:0801.4321 [hep-ph]], and references therein.
- [30] D. G. Cerdeño, C. Hugonie, D. E. Lopez-Fogliani, C. Muñoz and A. M. Teixeira, JHEP **0412** (2004) 048 [arXiv:hep-ph/0408102];
 D. G. Cerdeño, E. Gabrielli, D. E. Lopez-Fogliani, C. Muñoz and A. M. Teixeira, JCAP **0706** (2007) 008 [arXiv:hep-ph/0701271].
- [31] C. Hugonie, G. Belanger and A. Pukhov, JCAP **0711** (2007) 009 [arXiv:0707.0628 [hep-ph]].
- [32] A. Djouadi, U. Ellwanger and A. M. Teixeira, arXiv:0811.2699 [hep-ph].
- [33] S. A. Abel, S. Sarkar and P. L. White, Nucl. Phys. B **454** (1995) 663 [arXiv:hep-ph/9506359].
- [34] A. Menon, D. E. Morrissey and C. E. M. Wagner, Phys. Rev. D **70** (2004) 035005 [arXiv:hep-ph/0404184].
- [35] R. Kitano and K. y. Oda, Phys. Rev. D **61** (2000) 113001 [arXiv:hep-ph/9911327].
- [36] B. R. Greene and P. J. Miron, Phys. Lett. B **168** (1986) 226;
 R. Flores, K. A. Olive and D. Thomas, Phys. Lett. B **245** (1990) 509.
- [37] J. Dunkley *et al.* [WMAP Collaboration], Astrophys. J. Suppl. **180**, 306 (2009) [arXiv:0803.0586 [astro-ph]].
- [38] T. Nihei, L. Roszkowski and R. Ruiz de Austri, JHEP **0203** (2002) 031 [arXiv:hep-ph/0202009].
- [39] F. Domingo and U. Ellwanger, JHEP **0807** (2008) 079 [arXiv:0806.0733 [hep-ph]].
- [40] F. Domingo and U. Ellwanger, JHEP **0712** (2007) 090 [arXiv:0710.3714 [hep-ph]].

- [41] U. Ellwanger and C. Hugonie, *Comput. Phys. Commun.* **175**, 290 (2006); [arXiv:hep-ph/0508022]. G. Belanger, F. Boudjema, C. Hugonie, A. Pukhov and A. Semenov, *JCAP* **0509**, 001 (2005). [arXiv:hep-ph/0505142].
- [42] T. Aaltonen *et al.* [CDF Collaboration], *Phys. Rev. Lett.* **100** (2008) 101802 [arXiv:0712.1708 [hep-ex]].
- [43] V. M. Abazov *et al.* [D0 Collaboration], *Phys. Rev. D* **76** (2007) 092001 [arXiv:0707.3997 [hep-ex]].
- [44] E. Barberio *et al.* [Heavy Flavor Averaging Group (HFAG) Collaboration], arXiv:0704.3575 [hep-ex].
- [45] M. Misiak and M. Steinhauser, *Nucl. Phys. B* **764** (2007) 62 [arXiv:hep-ph/0609241]; M. Misiak *et al.*, *Phys. Rev. Lett.* **98** (2007) 022002 [arXiv:hep-ph/0609232].
- [46] Muon g-2 Collaboration, G. W. Bennett *et al.*, *Phys. Rev. Lett.* **92**, 161802 (2004) [arXiv:hep-ex/0401008].
- [47] T. Kinoshita and W. J. Marciano, in *Quantum Electrodynamics*, ed. T. Kinoshita (World Scientific, Singapore, 1990), p. 419;
T. Kinoshita, *Phys. Rev. Lett.* **75** (1995) 4728;
A. Czarnecki, B. Krause and W. J. Marciano, *Phys. Rev. Lett.* **76** (1996) 3267 [arXiv:hep-ph/9512369];
S. Eidelman and F. Jegerlehner, *Z. Phys. C* **67** (1995) 585 [arXiv:hep-ph/9502298];
K. Adel and F. J. Ynduráin, arXiv:hep-ph/9509378;
T. Kinoshita, B. Nizic and Y. Okamoto, *Phys. Rev. D* **31** (1985) 2108;
J. Bijnens, E. Pallante and J. Prades, *Phys. Rev. Lett.* **75** (1995) 1447 [Erratum-*ibid.* **75** (1995) 3781] [arXiv:hep-ph/9505251].
- [48] M. Davier, S. Eidelman, A. Höcker and Z. Zhang, *Eur. Phys. J. C* **31** (2003) 503 [arXiv:hep-ph/0308213];
K. Hagiwara, A. D. Martin, D. Nomura and T. Teubner, *Phys. Rev. D* **69**, 093003 (2004) [arXiv:hep-ph/0312250];
J. F. de Trocóniz and F. J. Ynduráin, *Phys. Rev. D* **71**, 073008 (2005) [arXiv:hep-ph/0402285].

- [49] T. Kinoshita and M. Nio, *Phys. Rev. D* **73** (2006) 053007 [arXiv:hep-ph/0512330]; K. Hagiwara, A. D. Martin, D. Nomura and T. Teubner, *Phys. Lett. B* **649** (2007) 173 [arXiv:hep-ph/0611102].
- [50] T. K. Gaisser, G. Steigman and S. Tilav, *Phys. Rev. D* **34**, 2206 (1986).
- [51] A. Bottino, N. Fornengo and S. Scopel, *Phys. Rev. D* **67** (2003) 063519 [arXiv:hep-ph/0212379].
- [52] A. Bottino, F. Donato, N. Fornengo and S. Scopel, *Phys. Rev. D* **69** (2004) 037302 [arXiv:hep-ph/0307303].
- [53] A. Bottino, F. Donato, N. Fornengo and S. Scopel, *Phys. Rev. D* **78** (2008) 083520 [arXiv:0806.4099 [hep-ph]].
- [54] C. E. Aalseth *et al.* [CoGeNT Collaboration], *Phys. Rev. Lett.* **101**, 251301 (2008) [arXiv:0807.0879 [astro-ph]].
- [55] G. Bertone, D. G. Cerdeño, J. I. Collar and B. C. Odom, *Phys. Rev. Lett.* **99** (2007) 151301 [arXiv:0705.2502 [astro-ph]].
- [56] W. S. Cho, K. Choi, Y. G. Kim and C. B. Park, *JHEP* **0802** (2008) 035 [arXiv:0711.4526 [hep-ph]].
- [57] W. S. Cho, K. Choi, Y. G. Kim and C. B. Park, arXiv:0810.4853 [hep-ph].
- [58] N. Okada and O. Seto, arXiv:0710.0449 [hep-ph].
- [59] F. Franke and H. Fraas, *Int. J. Mod. Phys. A* **12** (1997) 479 [arXiv:hep-ph/9512366].
- [60] M. Srednicki, R. Watkins and K. A. Olive, *Nucl. Phys. B* **310** (1988) 693.
- [61] J. L. Lopez, D. V. Nanopoulos and K. j. Yuan, *Phys. Rev. D* **48** (1993) 2766 [arXiv:hep-ph/9304216].
- [62] C. Amsler *et al.* [Particle Data Group], *Phys. Lett. B* **667** (2008) 1.
- [63] B. A. Dobrescu, G. L. Landsberg and K. T. Matchev, *Phys. Rev. D* **63** (2001) 075003 [arXiv:hep-ph/0005308]; B. A. Dobrescu and K. T. Matchev, *JHEP* **0009** (2000) 031 [arXiv:hep-ph/0008192].

- [64] J. F. Gunion, D. Hooper and B. McElrath, *Phys. Rev. D* **73** (2006) 015011 [arXiv:hep-ph/0509024].
- [65] R. Dermisek and J. F. Gunion, *Phys. Rev. Lett.* **95** (2005) 041801 [arXiv:hep-ph/0502105].
- [66] J. R. Ellis, A. Ferstl and K. A. Olive, *Phys. Lett. B* **481**, 304 (2000) [arXiv:hep-ph/0001005]; J. R. Ellis, A. Ferstl and K. A. Olive, *Phys. Rev. D* **63**, 065016 (2001) [arXiv:hep-ph/0007113]; J. R. Ellis, A. Ferstl and K. A. Olive, *Phys. Lett. B* **532**, 318 (2002) [arXiv:hep-ph/0111064].
- [67] A. Bottino, F. Donato, N. Fornengo and S. Scopel, *Astropart. Phys.* **13**, 215 (2000) [arXiv:hep-ph/9909228]. A. Bottino, F. Donato, N. Fornengo and S. Scopel, *Astropart. Phys.* **18**, 205 (2002) [arXiv:hep-ph/0111229].
- [68] J. R. Ellis, K. A. Olive, Y. Santoso and V. C. Spanos, *Phys. Rev. D* **71**, 095007 (2005) [arXiv:hep-ph/0502001].
- [69] J. Ellis, K. A. Olive and C. Savage, *Phys. Rev. D* **77** (2008) 065026 [arXiv:0801.3656 [hep-ph]].
- [70] L. Covi and S. Kraml, *JHEP* **0708** (2007) 015 [arXiv:hep-ph/0703130]; J. R. Ellis, K. A. Olive and Y. Santoso, *JHEP* **0810** (2008) 005 [arXiv:0807.3736 [hep-ph]].
- [71] J. R. Ellis, K. A. Olive and Y. Santoso, *JHEP* **0810**, 005 (2008) [arXiv:0807.3736 [hep-ph]].
- [72] J. McDonald, *Phys. Rev. D* **50** (1994) 3637 [arXiv:hep-ph/0702143];
- [73] C. P. Burgess, M. Pospelov and T. ter Veldhuis, *Nucl. Phys. B* **619** (2001) 709 [arXiv:hep-ph/0011335];
M. C. Bento, O. Bertolami, R. Rosenfeld and L. Teodoro, *Phys. Rev. D* **62** (2000) 041302 [arXiv:astro-ph/0003350];
M. C. Bento, O. Bertolami and R. Rosenfeld, *Phys. Lett. B* **518** (2001) 276 [arXiv:hep-ph/0103340];
H. Davoudiasl, R. Kitano, T. Li and H. Murayama, *Phys. Lett. B* **609** (2005) 117 [arXiv:hep-ph/0405097];
B. Patt and F. Wilczek, arXiv:hep-ph/0605188;
J. March-Russell, S. M. West, D. Cumberbatch and D. Hooper, *JHEP* **0807** (2008) 058 [arXiv:0801.3440 [hep-ph]].